

Bachelor's Thesis

# **Master Stability of Inertial Oscillator Networks with Delay**

**An analytical approach applied to  
renewable power grids**

Reyk Börner

Submitted in partial fulfillment of the Bachelor of Science  
at the

Department of Physics  
FREIE UNIVERSITÄT BERLIN

April 2019

*FU Supervisor:*

Prof. Dr. Petra Imhof  
Institute of Theoretical Physics  
Freie Universität Berlin

*PIK Supervisor:*

Dr. Frank Hellmann  
Potsdam Institute for Climate  
Impact Research (PIK)

*Second Assessor:*

Prof. Dr. Roland Netz  
Institute of Theoretical Physics  
Freie Universität Berlin

Contact: [reyk.boerner@fu-berlin.de](mailto:reyk.boerner@fu-berlin.de) or [reyk.boerner@online.de](mailto:reyk.boerner@online.de)

This edition contains minimal formatting and typographical changes made after submission.

## ABSTRACT

Time delays occur in a vast range of real-world dynamical systems due to finite reaction times or propagation speeds. Their influence on asymptotic behavior necessitates the consideration of delays in stability analysis. However, delay differential equations require subtle investigation because their characteristic equations generally feature an infinite-dimensional spectrum. Exact conditions for stability pose an open problem in research, particularly for complex systems. Here we derive an analytical approach to determine the linear stability of synchronous states in networks of coupled inertial oscillators with constant delay. Building on the master stability formalism, the method states necessary and sufficient delay stability conditions with respect to dynamical and structural parameters of the system. We apply the method to future power grids, where processing delays are expected to gain importance due to the ongoing transition to renewable energies. The study focusses on two conceptual models for frequency control, namely droop control and decentral smart grid control. Calculations based on simple network topologies show a critical delay for phase delays, while frequency delays lead to multiple stable regimes. The results suggest that increasing complexity diminishes delay stability, which underlines the relevance of delays in the design and control of real-world systems.

## ZUSAMMENFASSUNG

In nahezu allen dynamischen Systemen der realen Welt treten aufgrund von Reaktionszeiten oder endlichen Ausbreitungsgeschwindigkeiten Zeitverzögerungen auf. Diese *Delays* beeinflussen maßgeblich das asymptotische Verhalten und müssen daher in der Stabilitätsanalyse berücksichtigt werden. Allerdings bedürfen Delay-Differentialgleichungen einer subtilen Behandlung, da die zugehörigen charakteristischen Gleichungen ein unendliches Spektrum aufweisen. Die Suche nach exakten Stabilitätsbedingungen ist insbesondere im Gebiet der komplexen Systeme ein offenes Forschungsfeld. Kern dieser Arbeit ist die Herleitung einer analytischen Methode zur Bestimmung der linearen Stabilität synchroner Zustände in Netzwerken von gekoppelten trügen Oszillatoren mit konstanter Verzögerungszeit. Aufbauend auf dem Master-Stabilitäts-Formalismus erarbeiten wir notwendige und hinreichende Bedingungen für Delay-Stabilität in Abhängigkeit der dynamischen und strukturellen Parameter des Systems. Wir wenden die Methode auf zukünftige Stromnetze an, in denen Zeitverzögerungen im Zuge der Energiewende eine erwartbar zunehmende Rolle spielen werden. Die Betrachtung konzentriert sich auf zwei konzeptionelle Modelle zur Frequenzregelung (*droop control* sowie *decentral smart grid control*). Berechnungen auf einfachen Netzwerkstrukturen zeigen ein kritisches Delay für Verzögerungen in der Phase, während Verzögerungen in der Frequenz zu mehreren stabilen Bereichen führen. Die Ergebnisse deuten darauf hin, dass Systeme mit zunehmender Komplexität bei Zeitverzögerungen allgemein schneller instabil werden. Dies unterstreicht die Relevanz von Delays in der Planung und Regelung von realistischen dynamischen Systemen.

---

## Notation

$A, \mathcal{A}$	adjacency matrix; effective adjacency matrix
$Df$	Jacobian of the function $f$ evaluated at a fixed point $x^*$
$\tilde{d}_i$	effective weighted degree of the $i$ -th node
$\mathcal{D}$	effective weighted degree matrix
$\eta$	small displacement from a fixed point $x^*$ , $\eta = x - x^*$
$f_i^0, f^\tau$	functions of isolated node dynamics (no local delay; local processing delay)
$F^0 F^\tau$	global Jacobian matrix of $f_i^0, f^\tau$ (assumption 2)
$\mathcal{F}$	real part of the characteristic function
$g^{00}, g^{\tau\tau}, g^{0\tau}$	coupling functions (no coupl. delay; coupl. processing delay; commun. delay)
$G^{00}, G^{\tau\tau}, G^{0\tau}$	global (effective) Jacobian of $g^{00}, g^{\tau\tau}, g^{0\tau}$ (assumption 3)
$\mathcal{G}$	imaginary part of the characteristic function
$\mathcal{H}$	characteristic function of the linearized model
$h$	history function
$\mathbb{I}_{\mathbb{N}}$	$N$ -dimensional unit matrix
$K_{ij}$	coupling strength between nodes $i$ and $j$ (maximally transmittable power)
$L, \mathcal{L}$	Laplacian matrix; effective Laplacian matrix
$\lambda_k$	eigenvalue of $\mathcal{L}$ ( $\lambda_N$ : maximum eigenvalue; $\lambda_{min}$ : minimum eigenvalue in $\mathcal{N}$ )
$N$	system size (number of nodes)
$\bar{N}$	the set $\bar{N} = \{1, 2, \dots, N\}$
$\mathcal{N}$	transversal set
$\Omega$	global synchronization frequency
$\varpi_i$	second component of $\xi_i$ : angular frequency deviations from a fixed point
$P_i$	power production/consumption at node $i$ (+: production, -: consumption)
$\mathbb{R}^n, \mathbb{R}_{>0}$	$n$ -dimensional real coordinate space; set of all positive real numbers
$\text{Re}(z)$	real part of $z$
$\mathcal{S}$	complete synchronization manifold
$\tau$	constant time delay, $\tau > 0$
$\theta_i$	first component of $\xi_i$ : phase angle displacements from a fixed point
$w_{ij}$	weight factor that is pulled out of the coupling Jacobians (assumption 3)
$x, \dot{x}, \ddot{x}$	state vector $x = (x_1, x_2, \dots, x_N)^\top$ ; first and second derivatives by time $t$
$x^*$	fixed point
$x_i^\tau$	short notation for $x_i(t - \tau)$
$\xi$	small displacement from a fixed point in coordinates of the eigenspace of $\mathcal{L}$
$y_{1,k}, y_k^*, y_k^{**}$	roots of the real or imaginary part of the characteristic function, $\mathcal{F}$ or $\mathcal{G}$
$z$	root of the characteristic function $\mathcal{H}$
$\mathcal{Z}$	frequency synchronization manifold
$\otimes$	Kronecker product

---

Delay is preferable to error.  
*Thomas Jefferson*

# Contents

<b>1. Introduction</b>	<b>1</b>
<b>2. Stability of synchronization</b>	<b>2</b>
2.1. Linear stability analysis of nonlinear ODE systems . . . . .	2
2.2. Delay differential equations . . . . .	3
2.3. Synchronization in complex networks . . . . .	4
<b>3. Derivation of a delay master stability approach</b>	<b>6</b>
3.1. A delay model for coupled inertial oscillators . . . . .	6
3.1.1. Linearization near synchronous states . . . . .	7
3.2. Antisymmetric coupling: Processing delays . . . . .	8
3.2.1. The Laplacian $2 \times 2$ block decomposition . . . . .	8
3.2.2. Review: Bhatt-Hsu conditions for stability . . . . .	11
3.2.3. Delay master stability conditions . . . . .	12
3.3. Asymmetric coupling: Communication delays . . . . .	14
<b>4. Power grids as dynamical networks</b>	<b>16</b>
4.1. The power grid – today and tomorrow . . . . .	16
4.2. A complex network perspective . . . . .	18
4.2.1. Power flow . . . . .	19
4.2.2. The swing equation . . . . .	20
<b>5. Phase delay: Grid-forming inverters</b>	<b>21</b>
5.1. Droop-controlled inverter model with delay . . . . .	21
5.2. Delay master stability analysis . . . . .	21
5.3. Four-node star network . . . . .	23
5.4. Small-world networks . . . . .	26
<b>6. Frequency delay: Decentral smart grid control</b>	<b>29</b>
6.1. A delayed demand response model . . . . .	29
6.2. Delay master stability analysis . . . . .	29
6.3. Revisiting the star . . . . .	30
6.4. Back to the roots . . . . .	32
<b>7. Discussion</b>	<b>34</b>
<b>8. Conclusion and Outlook</b>	<b>36</b>
<b>Appendix</b>	<b>38</b>
<b>References</b>	<b>40</b>



# 1. Introduction

Anyone who has been stuck in traffic knows that time delays can cause desynchronization. The vehicles in front of you start moving, you happily accelerate, but seconds later you hit the break because the preceding vehicle stops down again. This loop repeats itself, creating an oscillatory motion commonly known as “stop and go.” Why don’t all vehicles advance with a common, constant speed? When one driver accelerates, it takes a certain time for the following driver to react. This creates elusive open spaces, motivating drivers to accelerate even more. Meanwhile, however, preceding vehicles congest because of going faster than the traffic density allowed, and to your frustration you must decelerate.

The time evolution of most real-world dynamical systems depends not only on the present state, but also on the past. This “memory effect” is induced by a delayed reaction of variables to changes in the system. Delays occur in nature and in engineered systems alike. In biology, for example, population dynamics depend on maturation and gestation times [1]. Processes in the Earth’s climate are affected by the time it takes mass or energy to propagate around the globe [2]. Furthermore, delays appear in the nervous system due to finite communication times between neurons and in lasers because of the finite speed of light [3–5]. Other examples include traffic control systems [6] or supply networks [7].

Our traffic jam example suggests that delays can qualitatively alter a system’s dynamical properties. Mathematically, we may describe a system with delay by a delay differential equation (DDE) [1, 8–12]. The first DDE was probably written around 1830 [3, 13], and the theory has been widely studied since the 1960s due to its interdisciplinary relevance. However, real-world systems with delay are typically difficult to tackle because of their high complexity. In fact, delays often arise from the manifold interactions between elements of the system. The relatively young theory of complex networks [14] provides a powerful framework to bring non-linear dynamics and complex interaction topologies together. As conceptual models that approximate many of the above examples, systems of coupled oscillators like the Kuramoto model [15] have attracted keen interest in the past years. In these models, the asymptotic stability of synchronous states is a central property with crucial implications for applications.

One of the most prominent real-world examples of a synchronized complex network is the power grid. Across continents, power units run on the same clock of a universal alternating current [16]. The world-wide increasing fraction of renewable energies in electricity production [17] requires the design of resilient, adaptive future energy systems. In contrast to conventional power plants, wind and solar energy sources are amorphously distributed across the grid [18, 19]. In addition, they produce highly volatile output on multiple timescales [20, 21]. To ensure stable operation despite increased complexity and heterogeneity of the system, control units must efficiently balance spatially and temporally fluctuating supply and demand. Grid-forming inverters, which interface distributed generation units and prosumers with the grid, have been identified as key actors in future energy systems [18]. In the absence of large synchronous generators with stabilizing rotational inertia, these control units take over the responsibility to maintain synchronization. Inevitably, they will need a certain time to measure and react to dynamical changes, which induces a delay in the network.

The question how delays affect the stability of synchronized oscillators is still an open research topic. Most studies have been limited to numerical analyses of characteristic equations or were restricted to simple network structures. Several papers [22–25] have analytically explored the limit of large delays in detail. In this thesis, we present an analytical approach to determine necessary and sufficient conditions for the stability of coupled inertial oscillator networks with any constant delay. Based on the master stability formalism by Pecora and Carroll [26], the derivation utilizes results of Bhatt and Hsu [27] who state stability criteria for second-order delay differential equations. We verify and illustrate the method by applying it to two different renewable power grid models.

## 2. Stability of synchronization

This section briefly illuminates relevant basics of dynamical systems theory and complex networks, setting the foundation for our subsequent study. First, we introduce the concept of linear stability analysis in the context of ordinary differential equations. We then extend this analysis to delay differential equations, before touching on the phenomenon of synchronization in oscillator networks.

### 2.1. Linear stability analysis of nonlinear ODE systems

The time evolution of a dynamical system is commonly represented by an autonomous ordinary differential equation (ODE) [28],

$$\dot{x}(t) = f(x(t)) , \quad (2.1)$$

where the vector  $x(t) \in \mathbb{R}^n$  characterizes a state of the system at time  $t$  and  $f : X \subseteq \mathbb{R}^n \rightarrow \mathbb{R}^n$  is some sufficiently nice differentiable function. All possible states of the system live in the finite-dimensional phase space  $X$  equipped with some norm  $\|\cdot\|$ . By specifying an initial condition,  $x(0) = x_0$ , a unique solution  $x(t; x_0)$  exists<sup>1</sup>, which we call a trajectory. Furthermore, we define a *fixed point*  $x^*$  as a state that satisfies the equation  $f(x^*) = 0$ . Fixed points represent equilibria of the system, as they do not change in time.

If  $f$  is a nonlinear function, exact solutions to (2.1) may be difficult or impossible to find. However, we can extract interesting information about the system by studying its asymptotic behavior as  $t \rightarrow \infty$ , without ever solving the ODE. A frequently asked question of dynamical systems theory concerns the attraction of fixed points: will a dissipative system, when slightly perturbed from an equilibrium, eventually return to this steady state and remain there forever?

Fixed points that locally attract trajectories are termed stable. Formally, we define stability in the following way [30].

**Definition 1** (Lyapunov stability). *A fixed point  $x^*$  is Lyapunov stable if for any  $\varepsilon > 0$  there exists a  $\delta > 0$  such that trajectories with initial conditions  $x_0$  in the neighborhood  $U_\varepsilon = \{x_0 : \|x_0 - x^*\| < \delta\}$  fulfill*

$$\|x(t; x_0) - x^*\| < \varepsilon \quad \forall t \geq 0 .$$

**Definition 2** (Asymptotic stability). *A Lyapunov stable fixed point  $x^*$  is asymptotically stable if all trajectories with  $x_0 \in U_\varepsilon$  converge to  $x^*$ , that is,*

$$\lim_{t \rightarrow \infty} \|x(t; x_0) - x^*\| = 0 .$$

Nonlinear systems may possess several stable fixed points (multistability). To analyze the effect of small displacements from an equilibrium, we linearize (2.1) around  $x^* = x - \eta$ , with  $\|\eta\|$  small:

$$\dot{\eta} \simeq f(x^*) + J(x^*)\eta + \mathcal{O}(\|\eta\|^2) , \quad (2.2)$$

where  $f(x^*) = 0$  by definition and  $J(x^*)$  denotes the Jacobian matrix of  $f$  evaluated at  $x^*$ . A basis of solutions to the linearized form is  $\eta(t) = \eta(0)e^{zt}$ , where  $z$  is a complex eigenvalue of  $J(x^*)$  and  $\eta(0)$  a corresponding eigenvector. For *asymptotic stability* it is sufficient that all eigenvalues have negative real parts, because if  $\text{Re}(z) < 0$  then  $\eta \rightarrow 0$  as  $t \rightarrow \infty$ . Equilibria of this type are called *linearly stable*. The determining eigenvalue  $z_{\max}$  with the largest real part is sometimes labeled *Lyapunov exponent*. Furthermore, it is necessary for asymptotic stability that the fixed point has no positive  $\text{Re}(z)$ . Only if an eigenvalue with  $\text{Re}(z) = 0$  exists, the answer about stability lies within higher order terms.

<sup>1</sup>For a proof of the existence and uniqueness of solutions of ODEs, see [28, 29].

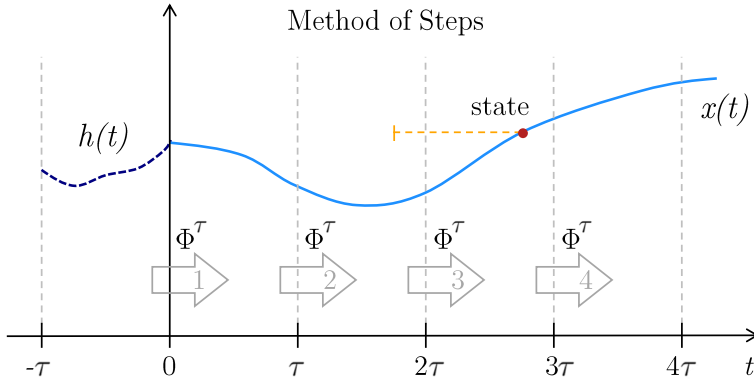


**Figure 1: Back to the future – the method of steps for DDEs.** Specification of a history function  $h$  in the interval  $[-\tau, 0]$  uniquely determines the solution in the interval  $[0, \tau]$ . Following solutions are found via step-by-step integration; the evolution operator  $\Phi^\tau$  maps a function in the previous interval to a function in the next  $\tau$ -interval. Note the possible discontinuity at  $t = 0$  between history function and trajectory [10]. The orange dotted line illustrates how far a system in a state at time  $t$  “remembers back”, leading to two interpretations of a state either as a discrete vector  $x(t)$  or a continuous function on the interval  $[t - \tau, t]$  [9].

Linear stability analysis thus allows us to investigate dynamical properties of a nonlinear system without explicitly solving the differential equations governing the system. Besides fixed points, a dynamical system may also have other asymptotic solutions (e.g. limit cycles, limit tori, strange attractors). Defining the stability of these solutions involves similar measures to the ones above, such that the ideas introduced here generally transfer. Below we will make use of the fact that under certain symmetry conditions especially limit cycles may be treated as fixed points.

## 2.2. Delay differential equations

The ODE presented above (2.1) assumes that the change of a state at time  $t$  depends exclusively on the state itself at that given time. If the system also depends on its past, we may describe its dynamics by a delay differential equation (DDE) – a differential equation with delayed time arguments. In the literature, DDEs are also referred to as differential-difference equations or retarded functional differential equations [8–10]. For a single, constant, and discrete delay  $\tau \in \mathbb{R}_{>0}$ , the general (autonomous) form of a DDE reads

$$\dot{x}(t) = f(x(t), x(t - \tau)) \quad (2.3)$$

This is the simplest case and the only one we consider here. Other DDEs feature more than one delay, time-dependent delays  $\tau(t)$ , state-dependent delays  $\tau(t, x(t))$ , or even more complicated non-discrete delays [11].

A solution of equation (2.3) is not uniquely determined by an initial condition  $x(0) = x_0$  because the trajectory is also affected by what happened in the system during the time interval  $[-\tau, 0]$ . Instead we must specify a *history function*  $h$  defined on  $[-\tau, 0]$  such that  $x(\zeta) = h(\zeta)$  for  $-\tau \leq \zeta \leq 0$ . To know how the system evolves from the state  $x(t)$ , we require knowledge of a “piece” of trajectory preceding the moment  $t$ , given by the mapping  $\zeta \mapsto x(t + \zeta; h)$  [9]. This leads to the *method of steps* which presents a solution approach for DDEs: using the history function, integrate (2.3) from  $t = 0$  to  $\tau$ . Then, take that solution as the “new” history function to determine the trajectory in the interval  $[\tau, 2\tau]$ , and so on (see fig. 1). The phase space of a delay system,  $X = C([-\tau, 0], \mathbb{R}^n)$ , is consequently an infinite-dimensional function space<sup>2</sup> [9, 10].

<sup>2</sup>Just like in the ODE case, we need some norm on  $X$  to define Lyapunov and asymptotic stability.

The infinite dimensionality of delay problems makes them more difficult to handle than finite-dimensional ODEs. Luckily, we can extend linear stability analysis to the more general delay case and gain insight into the asymptotic behavior of time-delayed systems [10, 12]. Let  $x^*$  be a fixed point<sup>3</sup> of (2.3) and  $\eta(t) = x(t) - x^*$  a small displacement. Similar to (2.2), linearization of (2.3) leads to

$$\dot{\eta}(t) \approx J_0(x^*)\eta(t) + J_\tau(x^*)\eta(t - \tau) , \quad (2.4)$$

where we again used the fact that  $f(x^*) = 0$ . Here, we have two Jacobians, both evaluated at the fixed point:  $J_0$  for the instantaneous  $x(t)$  and  $J_\tau$  for the delayed time argument. Substituting the ansatz  $\eta(t) = \eta(0)e^{zt}$  in (2.4), we obtain the *characteristic equation* of the fixed point,

$$\mathcal{H}(z, e^{-z\tau}) = \det(-z\mathbb{I}_n + J_0 + e^{-z\tau}J_\tau) = 0 . \quad (2.5)$$

$\mathbb{I}_n$  denotes the  $n$ -dimensional unit matrix. In the ODE case ( $J_\tau = 0$ ), the characteristic function  $\mathcal{H}$  is a polynomial with a finite number of roots – the  $n$  complex eigenvalues of the Jacobian  $J(x^*)$ . Here, we deal with a quasi-polynomial, or exponential polynomial, because  $z$  also appears as an exponent.  $\mathcal{H}$  given by (2.5) generally possesses an infinite number of complex roots [11]. The set of zeros constitutes the *spectrum* of equation (2.4); it extends infinitely in the negative direction of the real axis but is bounded in the positive direction [11]. If the entire spectrum lies strictly left of the imaginary axis, the corresponding fixed point is asymptotically stable [10, 31].

The central task of DDE linear stability analysis is thus to identify a *finite* subset of the spectrum containing all critical roots  $z$  that determine stability. Particularly for large interconnected systems, this remains an open research topic. Notable advances have recently been made analytically in the limit of large delays [22–25]. While this applies in some areas like optoelectronics, many complex systems feature delays on a time scale similar to their intrinsic dynamical time scales. In this case, the search for exact stability conditions continues.

### 2.3. Synchronization in complex networks

The mathematical abstraction of a network is a graph – a structure defined by a set of  $N$  nodes (vertices) and a set of  $M$  edges (links) [14]. Edges connect nodes to each other; they may be weighted or directed. The complete topological information of a graph is stored in its *adjacency matrix*  $A$ . For an undirected graph,

$$A_{ij} := \begin{cases} \ell_{ij} & \text{if nodes } i \text{ and } j \text{ are connected} \\ 0 & \text{else} \end{cases} , \quad (2.6)$$

where  $\ell_{ij} > 0$  is the weight of the edge between  $i$  and  $j$ . A closely related representation is the *graph Laplacian*  $L := D - A$ , by indices:

$$L_{ij} = \delta_{ij}\tilde{d}_i - A_{ij} , \quad \text{with } \tilde{d}_i = \sum_j A_{ij} . \quad (2.7)$$

Here,  $\delta_{ij}$  is the Kronecker delta;  $D$  denotes the diagonal matrix whose  $i$ -th diagonal entry corresponds to the weighted *degree*  $\tilde{d}_i$  of node  $i$ .  $L$  is symmetric and positive-semidefinite (for undirected graphs) because it has zero row-sum, meaning that its smallest eigenvalue is always  $\lambda_1 = 0$  [32].

The story becomes particularly interesting when we merge dynamical systems and networks in the study of *dynamics on networks*. This means that each node  $i$  accommodates a set of

<sup>3</sup>Here, we speak of states as vectors in  $\mathbb{R}^n$  given at time  $t$ , even though we formally introduced the phase space as a function space. These are merely two compatible interpretations of a state, as long as we keep in mind that DDE systems need a continuous initial condition  $h$  to be solved.

independent dynamical variables  $\{x_i, y_i, \dots\}$  interacting with variables  $\{x_j, y_j, \dots\}$  from other nodes  $j$  along the edges of the network [14].

In complex networks, the interactions between dynamical units cause the emergence of rich dynamical behavior. One of the most interesting and deeply studied emergent phenomena is synchronization [33]. In the most general sense, synchronization occurs when dynamical variables of all nodes start to do the same thing at the same time. But many systems in the real world do not behave in an arbitrary fashion; they follow a rhythm, from cycles of global climate to the periodic firing of neurons in a brain. It seems natural to model such processes by systems of coupled oscillators. Popular examples of synchronized oscillators include Huygen's pendulum clocks [33], flashing fireflies [34], coupled Josephson junctions [35] or pedestrians on the London Millennium Bridge [36].

In systems of  $N$  periodic oscillators<sup>4</sup>, synchronization refers to the locking of phases  $\phi_i$  for all  $i$ . Due to the coupling to each other or to a periodic external force, it is observed that all oscillators begin to oscillate with a common frequency. This phenomenon called frequency entrainment leads to a state of *frequency synchronization*<sup>5</sup> where phase differences between oscillators are constant. If also the phases align, we have *complete synchronization* [33].

In oscillator networks, linear stability analysis is concerned with the question whether a synchronous state is locally attractive, such that small perturbations cannot asymptotically destroy the synchronization. Apart from the trivial case of stagnant oscillators, a synchronous state forms a closed orbit in phase space (limit cycle). However, if in equilibrium all oscillators evolve with the same frequency  $\Omega$ , we can exploit this symmetry to reduce the problem to a more convenient study of fixed points with the help of a time-dependent coordinate shift:

$$\omega_i(t) = \omega'_i(t) - \Omega , \quad (2.8)$$

where the primed coordinates are in the inertial (time-independent) reference frame. Since the new reference frame co-rotates with the frequency  $\Omega$ , a state with synchronization frequency  $\Omega$  is a stationary state in the new coordinates. We note that the coordinate transform generates a degree of freedom  $\phi_0 \in [0, 2\pi)$  for the phases, which we may choose arbitrarily.

Before diving into our delay stability analysis, let us state an example of a coupled oscillator network. One of the most celebrated models in nonlinear sciences is the Kuramoto model [15],

$$\dot{\phi}_i = \omega_i + \frac{\kappa}{N} \sum_{j=1}^N \sin(\phi_j - \phi_i) , \quad i = 1, \dots, N . \quad (2.9)$$

Here,  $\phi_i$  is the phase of the  $i$ -th oscillator and  $\omega_i$  its natural frequency. This form considers all-to-all coupling with the homogenous coupling strength  $\kappa$ . The model has been used to describe many of the real-world systems mentioned above. A complex network version, extended to second order to include inertia, yields the second-order Kuramoto model [37, 38],

$$\ddot{\phi}_i = -\alpha_i \phi_i + \omega_i + \kappa \sum_{j=1}^N A_{ij} \sin(\phi_j - \phi_i) , \quad i = 1, \dots, N , \quad (2.10)$$

where  $\alpha_i$  denotes a damping parameter. The network topology enters via the adjacency matrix  $A = (A_{ij})$ .

Many studies focus on the special case of identical oscillators, i.e.  $\alpha_i = \alpha_0, \omega_i = \omega_0$ . Yeung and Strogatz [39] have studied time delays in the first-order Kuramoto model with mean-field coupling and noise. In this thesis, we investigate delays in second-order differential equations on a network structure. While our analysis is not restricted to the Kuramoto model but considers oscillator models more generally, equation (2.10) may serve as an illustrative example whenever needed. We will return to a very similar form in sections 5 and 6.

<sup>4</sup>Synchronization also occurs in chaotic oscillators; here we concentrate on the periodic case.

<sup>5</sup>Confusingly, frequency synchronization is sometimes referred to as phase synchronization [33].

### 3. Derivation of a delay master stability approach

In this section, we present a novel approach to analyze the linear stability of inertial oscillator networks with delay. Our derivation makes use of scalar delay stability conditions stated by Bhatt and Hsu in the 1960s [27] and builds on the master stability formalism (MSF) introduced by Pecora and Carroll in 1998 [26]. MSF yields conditions for the linear stability of  $N$  completely synchronized, identical coupled oscillators without delay. The general idea of our approach is to transfer this formalism to second-order DDEs in order to arrive at an expression that is compatible with Bhatt and Hsu's theorems. Unlike traditional MSF, we consider the more general case of frequency synchronization instead of complete synchronization.

The basic concept of MSF is to project the state vector of the linearized system into the eigenspace spanned by eigenvectors of the network's Laplacian matrix [32]. This results in a block form which allows to study the stability of the synchronous state as a function of the Laplacian eigenvalues. Instead of reviewing further details of the procedure, we demonstrate the steps by transferring them directly to our delay analysis. Results of Bhatt and Hsu are summarized in subsection 3.2.2.

#### 3.1. A delay model for coupled inertial oscillators

We consider a non-linear dynamical system of  $N$  coupled oscillators with inertia. Its time evolution is governed by a system of autonomous second-order differential equations. In a network context, each oscillator is a node, and weighted edges represent the coupling between them. The state of the  $i$ -th oscillator at time  $t$  is given by the vector  $x_i(t) = (\phi_i(t), \omega_i(t))^\top$ , which denotes the phase angle  $\phi_i$  and angular frequency deviation  $\omega_i = \dot{\phi}_i$  in a reference frame co-rotating with the natural frequency  $\Omega$  of the network (see section 2.3). We emphasize that although we treat  $\phi_i$  and  $\omega_i$  as two variables here<sup>6</sup>, they are not really independent ( $\omega_i$  is the time derivative of  $\phi_i$ ). Let  $f_i : \mathbb{R}^2 \rightarrow \mathbb{R}^2$  and  $g : \mathbb{R}^2 \times \mathbb{R}^2 \rightarrow \mathbb{R}^2$  be non-linear differentiable functions;  $g(x_i, x_i) = 0$ . If we assume that the time evolution of the system depends only on the present state, we can write, as an inertial oscillator model,

$$\dot{x}_i(t) = f_i(x_i(t)) + \sum_{j=1}^N A_{ij} g(x_i(t), x_j(t)) , \quad (3.1)$$

with  $i \in \bar{N} := \{1, \dots, N\}$ . Physically,  $f_i$  describes the isolated dynamics of the  $i$ -th node in the decoupled state, while the summation term characterizes contributions from other oscillators. The sum entails the time-independent weighted adjacency matrix  $A \in \mathbb{R}_{>0}^{N \times N}$ , which encodes the network structure, as well as the coupling function  $g$  describing the interaction between linked nodes. We require all oscillators to have equal damping and inertia constants. Nonetheless, the oscillators are not entirely identical because the functions  $f_i$  may differ from node to node due to distinct constant inhomogeneities  $c_i := (0, P_i)^\top$ ,  $P_i \in \mathbb{R}$ . These inhomogeneities account for local driving forces and make our model slightly more general than typical identical oscillator models. Limiting our study to undirected graphs without self-loops,  $A$  is symmetric and  $A_{ii} = 0 \forall i$ .

Let us now introduce a constant, discrete delay  $\tau > 0$  in the dynamics of model (3.1). This means that the change of the state vector  $x(t) = (x_1(t), x_2(t), \dots, x_N(t))^\top$  depends not only on the state vector at time  $t$  but also on the past state  $x(t - \tau)$ . In principle, a delayed time argument may occur in the isolated dynamics given by  $f_i$  as well as in any of the two arguments of the coupling function  $g$ . This motivates a breakdown into the following delay types:

- **Local processing delay,  $f^\tau(x_i(t - \tau))$**

Local processing delays occur when an oscillator at node  $i$  responds late to a local change at its position in the network. For instance, measuring the local phase or frequency and using the outcome of that measurement for feedback control induces a delayed reaction.

---

<sup>6</sup>The benefit of this description is that we can artificially write the problem in first-order differential form which is convenient for the first part of our derivation. Later, we return to second-order DDEs.

- **Coupling processing delay,**  $g^{\tau\tau}(x_i(t-\tau), x_j(t-\tau))$

Here, for any two linked oscillators  $i$  and  $j$ , the dynamical interaction is delayed. The state of the *edge* between them carries the delay, rather than the nodes individually. Again, control theory provides an example: if, say, the flow through an edge is measured, it takes at least the time of the measurement until the states of the adjacent nodes are adjusted.

- **Communication delay,**  $g^{0\tau}(x_i(t), x_j(t-\tau))$

Communication delays arise when considering finite propagation speeds of information, matter, or waves. The change of the  $i$ -th node depends on the history of connected nodes  $j$  because it took the time  $\tau$  for the signal or mass to travel from  $j$  to  $i$ .

We omit the fourth possible case, namely a reverse communication delay of the form

$$g^{\tau 0}(x_i(t-\tau), x_j(t)) ,$$

for the following two reasons. Firstly, the mathematical treatment would be similar to that of a communication delay. Secondly, we argue that it seems less intuitive: it would mean that the change at node  $i$  depends on what has been transmitted to other nodes and evaluated there, while information communicated to node  $i$  is instantaneous. Potential coupling functions of type  $g^\tau = g(x_j(t-\tau))$  are considered as special cases of a communication delay  $g^{0\tau}$ .

In addition to the delayed functions  $f^\tau$ ,  $g^{\tau\tau}$ , and  $g^{0\tau}$ , we further introduce the notation  $f_i^0$  and  $g^{00}$  for the undelayed functions  $f_i$  and  $g$ , respectively. Combining everything in one expression, we have a DDE inertial oscillator model,

$$\begin{aligned} \dot{x}_i &= f_i^0(x_i) + f^\tau(x_i^\tau) \\ &+ \sum_{j=1}^N A_{ij} \left( g^{00}(x_i, x_j) + g^{\tau\tau}(x_i^\tau, x_j^\tau) + g^{0\tau}(x_i, x_j^\tau) \right) , \end{aligned} \quad (3.2)$$

where we have abbreviated  $x_i \equiv x_i(t)$  and  $x_i^\tau \equiv x_i(t-\tau)$ .

Note that the vector  $x_i^\tau$  includes a delayed phase  $\phi_i(t-\tau)$  as well as a delayed frequency  $\omega_i(t-\tau)$ . Typically, models contain either delayed phases or delayed frequencies. For now, we combine both cases in  $x_i^\tau$ ; we will distinguish between them in section 3.2.2.

### 3.1.1. Linearization near synchronous states

To analyze the linear stability of model (3.2), we focus on its asymptotic behavior. Interesting candidates for stable solutions are synchronized periodic oscillations with a common frequency  $\Omega$ , which may be treated as a fixed point in a suitable co-rotating reference frame (see section 2.3). A tacit precondition of our delay analysis is that such a fixed point exists.

A fixed point  $x^* = (x_1^*, \dots, x_N^*)^\top$  is defined by the conditions  $\dot{x}_i^* = 0$  for all  $i$ . Since  $x_i^* = (\phi_i^*, \omega_i^*)^\top$  and  $\dot{\phi}_i^* = \omega_i^*$ , this directly implies  $\omega_i^* = 0$ . Physically, this means that all  $N$  oscillators run synchronously with frequency  $\Omega$  at all times, whereas they may not have equal phase angles. The set of fixed points is the *frequency synchronization manifold*  $\mathcal{Z}$  of the system,

$$\mathcal{Z} = \{x_i \in Z \subset \mathbb{R}^2 : i = 1, \dots, N \text{ and } \omega_i = 0 \forall i\} .$$

If, in addition to frequency synchronization, all phases are the same ( $\phi_i = \phi_0 \forall i$ ), the fixed point belongs to the *complete synchronization manifold*  $\mathcal{S} \subset \mathcal{Z}$ ,

$$\mathcal{S} = \{x_i \in S \subset \mathbb{R}^2 : i = 1, \dots, N \text{ and } \phi_i = \phi_0 \forall i\} .$$

We are interested in the dynamics of our delay model near the frequency synchronization manifold  $\mathcal{Z}$ . Substituting  $x_i = x_i^* + \eta_i$ , with  $||\eta_i||$  small for all  $i$ , the linearization of (3.2) yields

$$\dot{\eta}_i \approx D_i f^0 \eta_i + D_i f^\tau \eta_i^\tau \quad (3.3)$$

$$+ \sum_{j=1}^N A_{ij} \left[ \left( D_{ij}^1 g^{00} \eta_i + D_{ij}^2 g^{00} \eta_j \right) + \left( D_{ij}^1 g^{\tau\tau} \eta_i^\tau + D_{ij}^2 g^{\tau\tau} \eta_j^\tau \right) + \left( D_{ij}^1 g^{0\tau} \eta_i + D_{ij}^2 g^{0\tau} \eta_j^\tau \right) \right] ,$$

where Jacobian matrices, all evaluated at the fixed point, are written in short notation,

$$\mathrm{D}_i f := \left. \frac{\partial f(x_i)}{\partial x_i} \right|_{x_i=x_i^*}, \quad \mathrm{D}_{ij}^{1/2} g := \left. \frac{\partial g(x_i, x_j)}{\partial x_{i/j}} \right|_{x_i=x_i^*, x_j=x_j^*}$$

and  $\eta_i^\tau \equiv \eta_i(t - \tau)$ . To derive (3.3), we have utilized the fixed point solution,

$$0 = f_i^0(x_i^*) + f^\tau(x_i^*) + \sum_j A_{ij} \left( g^{00}(x_i^*, x_j^*) + g^{\tau\tau}(x_i^*, x_j^*) + g^{0\tau}(x_i^*, x_j^*) \right) \quad (3.4)$$

for all  $i \in \bar{N}$ . Note that the constant inhomogeneities  $c_i$  vanish when differentiating (hence we drop the index  $i$  of  $f_i^0$  in the linearized equation). All Jacobians in (3.3) are real  $2 \times 2$  matrices whose elements may depend on  $x_i^*$  (and  $x_j^*$ , in the coupling). Due to the relation  $\omega_i = \dot{\phi}_i$  between coordinates of the vector  $x_i$ , some elements of the Jacobians are immediately zero or one. Particularly,

$$\mathrm{D}_i f^0 = \begin{bmatrix} 0 & 1 \\ \partial_{\phi_i} f_2^0 & \partial_{\omega_i} f_2^0 \end{bmatrix}, \quad \mathrm{D}_i f^\tau = \begin{bmatrix} 0 & 0 \\ \partial_{\phi_i} f_2^\tau & \partial_{\omega_i} f_2^\tau \end{bmatrix}, \quad (3.5)$$

where  $\partial_m f_n$  denotes the partial derivative of the  $n$ -th component of the function  $f$  by the argument  $m$ , evaluated at the fixed point. In the same manner,

$$\mathrm{D}_{ij}^1 g^{00} = \begin{bmatrix} 0 & 0 \\ \partial_{\phi_i} g_2^{00} & \partial_{\omega_i} g_2^{00} \end{bmatrix}, \quad \mathrm{D}_{ij}^2 g^{00} = \begin{bmatrix} 0 & 0 \\ \partial_{\phi_j} g_2^{00} & \partial_{\omega_j} g_2^{00} \end{bmatrix}, \quad \text{etc.} \quad (3.6)$$

In the next section, we will consider the important special case of antisymmetric coupling, which allows us to reformulate the problem in an elegant form.

## 3.2. Antisymmetric coupling: Processing delays

So far, our study of the delay model (3.2) has been relatively general – we merely performed a linearization around synchronous states of the network. To continue along the path of the master stability formalism, we now concentrate on an asymmetric form of the coupling. This form commonly appears in flow and diffusion networks. Though we impose several restrictions, they are still fulfilled by many oscillator networks of interest.

### 3.2.1. The Laplacian $2 \times 2$ block decomposition

Consider the following assumption.

**Assumption 1** (Antisymmetric coupling). *The linearized coupling between two nodes  $i$  and  $j$  is antisymmetric, that is,*

i)  $D_{ij}^1 g(x_i^*, x_j^*) = -D_{ij}^2 g(x_i^*, x_j^*)$  and

ii) there is no communication delay.

Here,  $g$  is any of the coupling functions  $g^{00}$  or  $g^{\tau\tau}$ .

A simple, illustrative example for assumption 1 is the Kuramoto model (2.10), where the coupling function is

$$g^{00}(\phi_i, \phi_j) = \sin(\phi_j - \phi_i)$$

and thus  $D_{ij}^1 g^{00} = -D_{ij}^2 g^{00} = -\cos(\phi_j^* - \phi_i^*)$ .

Previous MSF studies have considered linearized models near the complete synchronization manifold  $\mathcal{S}$ . For identical oscillators in complete synchrony, the Jacobians are the same for all nodes  $i, j$  [26]. Then, the adjacency matrix  $A$  and the Jacobian  $Dg^{\tau\tau}$  (or  $Dg^{00}$ ) factorize into a

Kronecker product,  $A \otimes Dg^{\tau\tau}$  (or  $A \otimes Dg^{00}$ ). In other words, we can separate information about the global network structure from information about local dynamics between two nodes. This does not generally transfer to Jacobians evaluated on the frequency synchronization manifold  $\mathcal{Z}$ . However, the property is guaranteed by the following two restrictions.

**Assumption 2** (Homogeneity of local Jacobians). *The isolated  $2 \times 2$  Jacobians  $D_i f^0$ , evaluated on the frequency synchronization manifold  $\mathcal{Z}$ , are identical for all nodes:*

$$F^0 := D_1 f^0 = D_2 f^0 = \cdots = D_N f^0 .$$

Similarly, for the delayed isolated Jacobians,

$$F^\tau := D_1 f^\tau = D_2 f^\tau = \cdots = D_N f^\tau .$$

Then, the block-diagonal  $2N \times 2N$  matrix of all undelayed Jacobians  $D_i f^0$  factorizes into the Kronecker product  $\mathbb{I}_N \otimes F^0$ , where  $\mathbb{I}_N$  is the  $N$ -dimensional unit matrix<sup>7</sup>. For delayed Jacobians, assumption 2 leads to the factorization  $\mathbb{I}_N \otimes F^\tau$ . Considering identical oscillators, this is especially true if the functions  $f_i^0$  and  $f^\tau$  are linear functions of their arguments  $x_i$  and  $x_i^\tau$ , respectively (because then the derivatives are independent of  $x_i^*$ ).

**Assumption 3** (Factorizability of coupling Jacobians). *The adjacency matrix  $A$  and the Jacobian  $D_{ij}^2 g^{\tau\tau}$ , evaluated on the frequency synchronization manifold  $\mathcal{Z}$ , factorize into the direct product  $\mathcal{A} \otimes G^{\tau\tau}$  of an effective  $N \times N$  adjacency matrix  $\mathcal{A}$  and a universal  $2 \times 2$  Jacobian  $G^{\tau\tau}$ , such that the local matrix  $G^{\tau\tau}$  is the same for all nodes and only  $\mathcal{A}$  depends on the global indices  $i, j$  of the network. Like  $A$ , the effective adjacency matrix  $\mathcal{A}$  is symmetric and has no negative entries.*

In the case of undelayed coupling, the superscript  $\tau\tau$  is replaced by  $00$ .

In practice, assumption 3 means that we can pull a factor  $w_{ij}$  out of the Jacobian which contains all dependencies on  $x_i^*$  and  $x_j^*$ , and multiply this factor with the corresponding edge weight  $A_{ij}$  in order to obtain the effective weight  $\mathcal{A}_{ij} := w_{ij} A_{ij}$ .

To ease notation, we now focus on processing delays in the coupling (i.e.  $g^{00} = g^{0\tau} = 0$ ). The corresponding linearized model reads

$$\dot{\eta}_i \approx D_i f^0 \eta_i + D_i f^\tau \eta_i^\tau + \sum_{j=1}^N A_{ij} \left( D_{ij}^1 g^{\tau\tau} \eta_j^\tau + D_{ij}^2 g^{\tau\tau} \eta_j^\tau \right) . \quad (3.7)$$

The subsequent decomposition works equally well for undelayed coupling, i.e.  $g^{0\tau} = g^{\tau\tau} = 0$ . We present results for both cases at the end of the derivation. In fact, as long as both functions  $g^{00}$  and  $g^{\tau\tau}$  fulfill assumptions 1 and 3, sums of the two coupling functions are possible as well. However, regarding assumption 3, the Jacobians  $D_{ij}^2 g^{00}$  and  $D_{ij}^2 g^{\tau\tau}$  must then lead to the same effective adjacency matrix  $\mathcal{A}$  which might not be the case in practice.

Now, assumptions 1 and 3 imply that for  $i, j \in \bar{N}$  and  $m, n \in \{1, 2\}$ , the coupling sum can be rewritten as

$$\sum_{j,n} \mathcal{A}_{ij} G_{mn}^{\tau\tau} (\eta_{jn}^\tau - \eta_{in}^\tau) = \sum_{j,n} \mathcal{A}_{ij} G_{mn}^{\tau\tau} \eta_{jn}^\tau - \tilde{d}_i \sum_n G_{mn}^{\tau\tau} \eta_{in}^\tau , \quad (3.8)$$

where  $\tilde{d}_i := \sum_j \mathcal{A}_{ij}$  is the effective weighted degree of node  $i$  and  $\eta_{jn}$  denotes the  $n$ -th component of  $\eta_j$ . Equation (2.7) allows us to rewrite (3.7) in terms of the (effective) graph Laplacian  $\mathcal{L}$ :

$$\dot{\eta}_i = F^0 \eta_i + F^\tau \eta_i - \sum_{j=1}^N \mathcal{L}_{ij} G^{\tau\tau} \eta_j^\tau , \quad (3.9)$$

<sup>7</sup>Technically, assumption 2 is slightly more restrictive than necessary. The cases that we exclude by this, however, are probably not very realistic. This is discussed further in section 7.

or, in vector notation for the entire system,  $\eta = (\eta_1, \dots, \eta_N)^\top$ ,

$$\dot{\eta} = [\mathbb{I}_N \otimes F^0]\eta + [\mathbb{I}_N \otimes F^\tau]\eta^\tau - [\mathcal{L} \otimes G]\eta^\tau . \quad (3.10)$$

With assumption 3,  $\mathcal{A}$  and  $\mathcal{L}$  are symmetric and therefore diagonalizable. Since the Laplacian matrix of an undirected graph is positive-semidefinite, its smallest eigenvalue is  $\lambda_1 = 0$ . Switching to a basis  $\mathcal{B}$  of eigenvectors via the coordinate transform  $\xi = [T_{\mathcal{B}} \otimes \mathbb{I}_2]\eta$ , we can rewrite  $\mathcal{L} = T_{\mathcal{B}}^{-1}\Lambda T_{\mathcal{B}}$  as a diagonal matrix of its eigenvalues,  $\Lambda = \text{diag}(\lambda_1, \dots, \lambda_N)$ :

$$\dot{\xi} = [\mathbb{I}_N \otimes F^0]\xi + [\mathbb{I}_N \otimes F^\tau]\xi^\tau - [\Lambda \otimes G^{\tau\tau}]\xi^\tau . \quad (3.11)$$

Eq. (3.11) has a block-diagonal form; consequently, the problem splits up into  $N$  two-dimensional blocks, each given by the equation

$$\dot{\xi}_k = F^0\xi_k + (F^\tau - \lambda_k G^{\tau\tau})\xi_k^\tau , \quad k \in \bar{N} . \quad (3.12)$$

In the case of undelayed coupling ( $g^{00}$ ), an analogous procedure leads to

$$\dot{\xi}_k = (F^0 - \lambda_k G^{00})\xi_k + F^\tau\xi_k^\tau , \quad k \in \bar{N} , \quad (3.13)$$

with possibly different eigenvalues<sup>8</sup>  $\lambda_k$ .

We have switched index from  $i$  to  $k$  to emphasize that  $\xi$  represents the state vector in the eigenbasis  $\mathcal{B}$ . Its components  $\xi_k = (\theta_k, \varpi_k)^\top$  contain the phases  $\theta_k$  and angular frequency deviations  $\varpi_k = \dot{\theta}_k$  in the transformed coordinates. Specifically, with respect to  $\mathcal{B}$ , the vector  $\phi$  of all phase angles is given by the linear combination

$$\phi = \sum_k v_k \theta_k , \quad (3.14)$$

where  $v_k$  is an eigenvector of  $\mathcal{L}$ .

**Second-order DDE form.** Inertial oscillators are commonly described by second-order differential equations. So far, we have written the problem in first-order form by interpreting  $\omega_i = \dot{\phi}_i$  as a second variable at each node  $i$ . Now that we have decomposed the network model into a set of block equations, let us rewrite the blocks (3.12) respectively (3.13) as second-order DDEs,

$$\ddot{\theta}_k = -a_k \dot{\theta}_k - b_k \theta_k - s_{1,k} \dot{\theta}_k^\tau - s_{0,k} \theta_k^\tau , \quad (3.15)$$

where  $k \in \bar{N}$  and the (small) phase angles  $\theta_k$  are given via (3.14). For a *coupling processing delay* ( $g^{00} = g^{0\tau} = 0$ ), the coefficients in (3.15) are given by

$$\begin{aligned} a_k &= -F_{22}^0 & s_{1,k} &= -F_{22}^\tau + \lambda_k G_{22}^{\tau\tau} \\ b_k &= -F_{21}^0 & s_{0,k} &= -F_{21}^\tau + \lambda_k G_{21}^{\tau\tau} . \end{aligned} \quad (3.16)$$

In the case of *undelayed coupling* ( $g^{0\tau} = g^{\tau\tau} = 0$ ), the coefficients become

$$\begin{aligned} a_k &= -F_{22}^0 + \lambda_k G_{22}^{00} & s_{1,k} &= -F_{22}^\tau \\ b_k &= -F_{21}^0 + \lambda_k G_{21}^{00} & s_{0,k} &= -F_{21}^\tau . \end{aligned} \quad (3.17)$$

In the spirit of the master stability formalism [26], we have arrived at an expression (3.15), with coefficients according to either (3.16) or (3.17), where the  $k$ -dependency rests solely in the eigenvalue  $\lambda_k$ . Note that the second-order form distinguishes between delays in the phase  $\theta_k^\tau$  and delays in the frequency  $\varpi_k^\tau = \dot{\theta}_k^\tau$  of the oscillators. Many delay models of interest fulfill the following assumption.

---

<sup>8</sup>Remember that  $\lambda_k$  is an eigenvalue of the *effective* Laplacian matrix containing fixed point dependent weights. Therefore, the eigenvalues do not depend exclusively on the network structure but also on the coupling dynamics.

**Assumption 4** (Single delay term). *The delay  $\tau$  in model (3.2) appears either exclusively in the phase or exclusively in the frequency, such that one of the following situations pertains for all  $k \in \bar{N}$ :*

- i)  $s_{1,k} = 0$  and  $s_{0,k} \neq 0$  (phase delay) or
- ii)  $s_{0,k} = 0$  and  $s_{1,k} \neq 0$  (frequency delay).

Under assumptions 1-4, we can now adopt theorems presented by Bhatt and Hsu [27] to state necessary and sufficient conditions for the linear stability of model (3.2). In the following, we review the key results of [27].

### 3.2.2. Review: Bhatt-Hsu conditions for stability

Bhatt and Hsu investigate second-order DDEs of the form

$$0 = m\ddot{\theta}(t) + a\dot{\theta}(t) + b\theta(t) + s_n \frac{d^n\theta(t-\tau)}{dt^n}, \quad (3.18)$$

where  $n \in \{0, 1, 2\}$ ; the constants  $m, a, b, s_n \in \mathbb{R}$  and  $\tau > 0$ . (Notice the similarity between this equation (3.18) and a single block of (3.15) under assumption 4.) With the change of coordinates  $t = \tau\zeta$  we get, in terms of the normalized time  $\zeta$ ,

$$0 = \ddot{\theta}(\zeta) + p\dot{\theta}(\zeta) + q\theta_k(\zeta) + r_n \frac{d^n\theta(\zeta-1)}{d\zeta^n}, \quad (3.19)$$

where

$$p = \frac{a}{m}\tau, \quad q = \frac{b}{m}\tau^2, \quad r_n = \frac{s_n}{\mu}\tau^{2-n}. \quad (3.20)$$

Furthermore, the characteristic equation of (3.19) is

$$\mathcal{H}(z, e^z) := (z^2 + pz + q)e^z + r_n z^n = 0. \quad (3.21)$$

Substituting  $z = iy$ , where we denote by  $i$  the imaginary unit, the characteristic polynomial separates into a real and an imaginary part,

$$\mathcal{H}(iy) = \mathcal{F}(y) + i\mathcal{G}(y). \quad (3.22)$$

An equilibrium point is linearly asymptotically stable if and only if all roots of the exponential polynomial  $\mathcal{H}$  have negative real parts (see section 2.2). A theorem by Pontrjagin [40, 41] ensures this requirement by imposing necessary and sufficient conditions on the roots of  $\mathcal{G}(y)$  and  $\mathcal{F}(y)$ . In [27], Bhatt and Hsu expand on Pontrjagin's theorem by conducting a case study for different  $n$  as well as different values of  $p$  and  $q$ . For each combination, they identify which roots  $y_i$  govern the stability of the system, and express upper and lower bounds in terms of these roots. Here, we focus on two of those cases:

- I. Let  $n = 0$ ,  $p > 0$  and  $-p < q \leq 0$  (subcase 1C in [27]). Then, the imaginary part of the characteristic polynomial  $\mathcal{G}(y)$ ,

$$\mathcal{G}(y) = (q - y^2) \sin y + py \cos y, \quad (3.23)$$

has precisely one root  $y_1$  in the interval  $(0, \pi]$ . Bhatt and Hsu derive the following theorem:

**Theorem 1.** *Let  $n = 0$ ,  $p > 0$  and  $-p < q \leq 0$ . A system governed by (3.18) is linearly asymptotically stable if and only if*

$$-q < r_0 < R(y_1) := \sqrt{(y_1^2 - q)^2 + p^2 y_1^2}. \quad (3.24)$$

**II.** Let  $n = 1$ ,  $p > 0$  and  $q > 0$  (subcase 2A in [27]). For this case, we consider roots of the real part of the characteristic equation,

$$\mathcal{F}(y) = (q - y^2) \cos y - py \sin y . \quad (3.25)$$

$\mathcal{F}(y)$  possesses a root  $y_0$  in the interval  $(0, \pi/2)$  and one root  $y_j$  in each of the following  $\pi$ -intervals  $(j\pi - \pi/2, j\pi + \pi/2)$  for  $j = 1, 2, \dots$ . If  $j$  is even/odd, let us call  $y_j$  an even/odd root. Of all even roots and, respectively, of all odd roots, we need to find the root  $y^{**}$ , respectively  $y^*$ , which yields the smallest value  $\Delta_j = |y_j - \sqrt{q}|$ . Then, Bhatt and Hsu state the following condition:

**Theorem 2.** *Let  $n = 1$ ,  $p > 0$  and  $q > 0$ . A system governed by (3.18) is linearly asymptotically stable if and only if*

$$-\frac{R(y^{**})}{y^{**}} < r_1 < \frac{R(y^*)}{y^*} \quad (3.26)$$

with  $R(y) = \sqrt{(y^2 - q)^2 + p^2 y^2}$ .

### 3.2.3. Delay master stability conditions

After this brief review, let us transfer the results to our oscillator network. While theorems 1 and 2 hold for one-dimensional systems, we deal with  $N$  blocks for the phases of  $N$  oscillators here. Under assumption 4, each  $k$ -block of (3.15) has the second-order DDE form studied by Bhatt and Hsu (3.18). The coefficients  $a_k, b_k, s_{n,k}$  relate to the normalized Bhatt-Hsu coefficients  $p, q, r_n$  via

$$p \leftrightarrow a_k \tau, \quad q \leftrightarrow b_k \tau^2, \quad r_1 \leftrightarrow s_{1,k} \tau, \quad r_0 \leftrightarrow s_{0,k} \tau^2 . \quad (3.27)$$

With these relations, we can state stability conditions for any block, as a function of  $\lambda_k$  and  $\tau$ . We argue that a synchronized state of (3.2), under the proposed assumptions, is linearly asymptotically stable if and only if the appropriate Bhatt-Hsu condition in [27] is fulfilled for all  $k$  in the *transversal set*  $\mathcal{N}$ .

**Definition 3** (Transversal set). *The transversal set  $\mathcal{N}$  is defined as*

$$\mathcal{N} := \begin{cases} \{2, \dots, N\} & f^\tau = 0 \\ \{1, \dots, N\} & f^\tau \neq 0 \end{cases} \quad (3.28)$$

If the delay appears exclusively in the coupling ( $f^\tau = 0$ ), the eigenvalue  $\lambda_1 = 0$  does not affect the stability because it describes dynamics within the frequency synchronization manifold  $\mathcal{Z}$ . All other  $k$  represent transversal directions which need to be stable to remain in the synchronization manifold [26]. In contrast, local delays ( $f^\tau \neq 0$ ) do not vanish in the block  $k = 1$ ; therefore we must consider all  $k \in \bar{\mathcal{N}}$  for this case. Our stability analysis is thus based on  $N - 1$  or  $N$  conditions.

We are now ready to formulate the following delay stability conditions:

**Case I: Phase delay.** Consider assumptions 1-3. If additionally assumption 4 (i) holds, the change of the system at time  $t$  depends on the phase angle deviations  $\theta_k$  of all oscillators at an earlier instant  $t - \tau$ . We further require  $a_k > 0$  and  $-a_k < b_k \tau \leq 0$ . Then, the imaginary part of the characteristic polynomial  $\mathcal{G}_k(y)$  has precisely one root  $y_{1,k}$  in the interval  $(0, \pi]$ . Theorem 1 implies the following stability condition.

**Stability condition 1** (Phase delay). *Let  $a_k > 0$  and  $-a_k < b_k \tau \leq 0$  under assumption 4 (i). A system governed by (3.2) is linearly asymptotically stable if and only if*

$$-b_k < s_{0,k} < \frac{R(y_{1,k})}{\tau^2} \quad (3.29)$$

with  $R(y_{1,k}) = \sqrt{(y_{1,k}^2 - b_k \tau^2)^2 + (a_k \tau y_{1,k})^2}$

for all  $k \in \mathcal{N}$ .

As it turns out, it may suffice in practice to test only the largest eigenvalue  $\lambda_N$  instead of all blocks in the transversal set. For a coupling processing delay with coefficients given in (3.16), the root  $y_{1,k}$  is independent of  $k$  and stability condition 1 is specifically

$$(F_{21}^0 + F_{21}^\tau) < \lambda_k G_{21}^{\tau\tau} < \frac{R(y_1)}{\tau^2} \quad (3.30)$$

with  $R(y_1) = \sqrt{(y_1^2 + \tau^2 F_{21}^0)^2 + (y_1 \tau F_{22}^0)^2}$ .

The inequalities impose lower and upper bounds for possible values of  $\lambda_k \in \mathcal{N}$ . Since the eigenvalues are ordered,  $\lambda_1 < \lambda_2 < \dots < \lambda_N$ , we merely have to test the extreme ends of the transversal set, i.e.  $k = N$  and either  $k = 1$  or  $k = 2$ . This yields the conditions

$$\begin{aligned} G_{21}^{\tau\tau} > 0 \quad \Rightarrow \quad \lambda_{min} > \frac{F_{21}^0 + F_{21}^\tau}{G_{21}^{\tau\tau}} \quad \text{and} \quad \lambda_N < \frac{F_{21}^\tau}{G_{21}^{\tau\tau}} + \frac{R(y_1)}{\tau^2 G_{21}^{\tau\tau}} \\ G_{21}^{\tau\tau} < 0 \quad \Rightarrow \quad \lambda_{min} < \frac{F_{21}^0 + F_{21}^\tau}{G_{21}^{\tau\tau}} \quad \text{and} \quad \lambda_N > \frac{F_{21}^\tau}{G_{21}^{\tau\tau}} + \frac{R(y_1)}{\tau^2 G_{21}^{\tau\tau}} \end{aligned} \quad (3.31)$$

where  $\lambda_{min}$  denotes the smallest eigenvalue included in the transversal set. Note that the inequalities involving  $\lambda_{min}$  are independent of  $\tau$ ; they express a necessary stability condition regardless of the delay. Once this criterion is fulfilled, the delay-dependent stability of the synchronous state is determined by the *delay master stability condition*

$$\lambda_N < \frac{F_{21}^\tau}{G_{21}^{\tau\tau}} + \frac{1}{\tau^2 G_{21}^{\tau\tau}} \sqrt{(y_1^2 + \tau^2 F_{21}^0)^2 + (y_1 \tau F_{21}^0)^2} \quad (3.32)$$

for  $G_{21}^{\tau\tau} > 0$ . The associated *delay master stability function*  $\sigma(\lambda_N, \tau)$  reads

$$\sigma(\lambda_N, \tau) = \lambda_N - \frac{F_{21}^\tau}{G_{21}^{\tau\tau}} - \frac{1}{\tau^2 G_{21}^{\tau\tau}} \sqrt{(y_1(\tau)^2 + \tau^2 F_{21}^0)^2 + (y_1(\tau) \tau F_{21}^0)^2}. \quad (3.33)$$

The system is linearly asymptotically stable only in the regions where  $\sigma < 0$ . We continue our analysis of this case in section 5 by means of an example. The case of undelayed coupling with phase delay is not expanded in further detail here.

**Case II: Frequency delay.** If, besides assumptions 1-3, assumption 4 (ii) holds, the dynamical change of the system (3.2) at time  $t$  depends on past frequency deviations at  $t - \tau$ . We require  $a_k > 0$  and  $b_k > 0$ . For this case, we consider roots of the real part of the characteristic equation.  $\mathcal{F}_k(y)$  possesses a root  $y_{0,k}$  in the interval  $(0, \pi/2)$  and one root  $y_{j,k}$  in each of the following  $\pi$ -intervals  $(j\pi - \pi/2, j\pi + \pi/2)$  for  $j = 1, 2, \dots$ . If  $j$  is even/odd, let us call  $y_{j,k}$  an even/odd root. Of all even roots and, respectively, of all odd roots, we need to find the root  $y_k^{**}$ , respectively  $y_k^*$ , which yields the smallest value  $\Delta_{j,k} = |y_{j,k} - \sqrt{b_k \tau^2}|$ . Then, theorem 2 yields the following condition.

**Stability condition 2** (Frequency delay). *Let  $a_k > 0$  and  $b_k > 0$  under assumption 4 (ii). A system governed by (3.2) is linearly asymptotically stable if and only if*

$$-\frac{R_k(y_k^{**})}{y_k^{**}} < s_{1,k}\tau < \frac{R_k(y_k^*)}{y_k^*} \quad (3.34)$$

with  $R_k(y_k) = \sqrt{(y_k^2 - b_k \tau^2)^2 + (a_k \tau y_k)^2}$

for all  $k \in \mathcal{N}$ .

Note that the left side of stability condition 2 is always negative, whereas the right side is always positive. Hence, if we know the sign of  $s_{1,k}$ , we must only check one of the two inequalities. Finding the right roots  $y^*$  and  $y^{**}$  appears somewhat less straightforward than in the phase

delay case. However, for a given delay, we know where to look for them: assume the value  $\sqrt{b_k \tau^2}$  is located in the interval  $(j\pi - \pi/2, j\pi + \pi/2)$ , where  $j$  is a positive integer. If  $j$  is an odd number, the closest root is in the same interval. Otherwise, we find  $y_k^*$  in the  $\pi$ -interval to the right ( $j+1$ ) or to the left ( $j-1$ ). This implies that if we “look” to the right and left of the value  $\sqrt{b_k \tau^2}$  up to a distance of  $3\pi/2$ , we find at minimum one and at maximum two roots. Thus, we must compute  $2N$  roots in the worst case. In section 6, we look at frequency delays more elaborately in the context of a local processing delay example.

### 3.3. Asymmetric coupling: Communication delays

The derivation above relies on the assumption of antisymmetric coupling between connected nodes  $i$  and  $j$  (assumption 1). For some inertial oscillator models, this may not be valid. In particular, a communication delay immediately destroys the antisymmetry because the coupling function  $g^{0\tau}(x_i, x_j^\tau)$  evaluates its arguments at different times. We comprise all non-antisymmetric coupling functions in the term “asymmetric”, although this includes symmetric forms as well.

To decompose the asymmetric problem into blocks like in the previous case, let us first update assumption 3 to a new version:

**Assumption 5** (Factorizability of asymmetric coupling Jacobians). *Let  $g$  denote any of the coupling functions  $g^{00}, g^{0\tau}$ , or  $g^{\tau\tau}$ . The adjacency matrix  $A$  and the Jacobian  $D_{ij}^2 g(x_i^*, x_j^*)$ , evaluated on the frequency synchronization manifold  $\mathcal{Z}$ , factorize into the direct product  $\mathcal{A} \otimes G^{(2)}$  of an effective  $N \times N$  adjacency matrix  $\mathcal{A}$  and a universal  $2 \times 2$  Jacobian  $G^{(2)}$ , such that the local matrix  $G^{(2)}$  is the same for all nodes and only  $\mathcal{A}$  depends on the global indices  $i, j$  of the network.*

Similarly,  $A$  and  $D_{ij}^1 g(x_i^*, x_j^*)$  factorize into the direct product  $\mathcal{A}' \otimes G^{(1)}$ .  $\mathcal{A}$  and  $\mathcal{A}'$  are symmetric matrices like  $A$ .

Consider a situation in which assumptions 2, 4, and 5 apply but 1 fails. Then, we cannot switch into the eigenbasis of the Laplacian matrix  $\mathcal{L}$  as performed in section 3.2. But since  $\mathcal{A}$  and  $\mathcal{A}'$  are diagonalizable as well (we required them to be symmetric), there is another way. It comes at a price, since we need the following rather restrictive assumption:

**Assumption 6** (Simultaneous diagonalizability). *The weighted degree matrix  $\mathcal{D}$  defined by*

$$\mathcal{D}_{ij} := \begin{cases} \tilde{d}_i := \sum_l \mathcal{A}'_{il} & \text{if } j = i \\ 0 & \text{otherwise} \end{cases} \quad i, j, l \in \bar{N}$$

and the effective adjacency matrix  $\mathcal{A}$  commute, that is,

$$[\mathcal{D}, \mathcal{A}] = 0 .$$

This implies that the linear transformation  $T_{\mathcal{A}}$  diagonalizing  $\mathcal{A}$  leaves  $\mathcal{D}$  diagonalized (simultaneous diagonalizability). Since the diagonal elements  $\mathcal{D}_{ii}$  correspond to weighted degrees  $\tilde{d}_i$  of node  $i$ , assumption 6 is automatically valid for regular graphs with homogenous weights.  $\mathcal{D}$  is then proportional to the unit matrix. More complex network topologies generally do not satisfy assumption 6.

We now focus on communication delays to derive the asymmetric case. The communication delay model, potentially with a processing delay in the isolated dynamics, reads

$$\dot{\eta}_i \approx D_i f^0 \eta_i + D_i f^\tau \eta_i^\tau + \sum_{j=1}^N A_{ij} \left( D_{ij}^1 g^{0\tau} \eta_i + D_{ij}^2 g^{0\tau} \eta_j^\tau \right) . \quad (3.35)$$

In contrast to eq. (3.8), we now have, for  $i, j \in \bar{N}$  and  $m, n \in \{1, 2\}$ ,

$$\sum_{jn} \left( \mathcal{A}'_{ij} G_{mn}^{(1)} \eta_{in} + \mathcal{A}_{ij} G_{mn}^{(2)} \eta_{jn}^\tau \right) = \tilde{d}_i \sum_n G_{mn}^{(1)} \eta_{in} + \sum_{jn} \mathcal{A}_{ij} G_{mn}^{(2)} \eta_{jn}^\tau . \quad (3.36)$$

Using assumption 6, let  $\Upsilon = T_{\mathcal{A}} \mathcal{D} T_{\mathcal{A}}^{-1} =: \text{diag}(v_1, \dots, v_N)$  and  $\Gamma = T_{\mathcal{A}} \mathcal{A} T_{\mathcal{A}}^{-1} =: \text{diag}(\rho_1, \dots, \rho_N)$ . Then,

$$\dot{\xi} = [\mathbb{I}_N \otimes F^0] \xi + [\mathbb{I}_N \otimes F^\tau] \xi^\tau + [\Upsilon \otimes G^{(1)}] \xi + [\Gamma \otimes G^{(2)}] \xi^\tau , \quad (3.37)$$

which we may write in block form,

$$\dot{\xi}_k = (F^0 + v_k G^{(1)}) \xi_k + (F^\tau + \rho_k G^{(2)}) \xi_k^\tau . \quad (3.38)$$

As before, we can use  $\varpi_k = \dot{\theta}_k$  to write (3.38) in second-order form:

$$\ddot{\theta}_k = a_k \dot{\theta}_k + b_k \theta_k + s_{1,k} \dot{\theta}_k^\tau + s_{0,k} \theta_k^\tau , \quad (3.39)$$

where  $k \in \bar{N}$  and the coefficients are given by

$$\begin{aligned} a_k &= F_{22}^0 + v_k G_{22}^{(1)} & s_{1,k} &= F_{22}^\tau + \rho_k G_{22}^{(2)} \\ b_k &= F_{21}^0 + v_k G_{21}^{(1)} & s_{0,k} &= F_{21}^\tau + \rho_k G_{21}^{(2)} . \end{aligned} \quad (3.40)$$

Invoking assumption 4, we can once again identify the block equation (3.39) with the form studied by Bhatt and Hsu (see section 3.2.2). This allows us to state necessary and sufficient conditions for linear stability of inertial oscillator networks with communication delay, albeit under the hypothetical assumption 6.

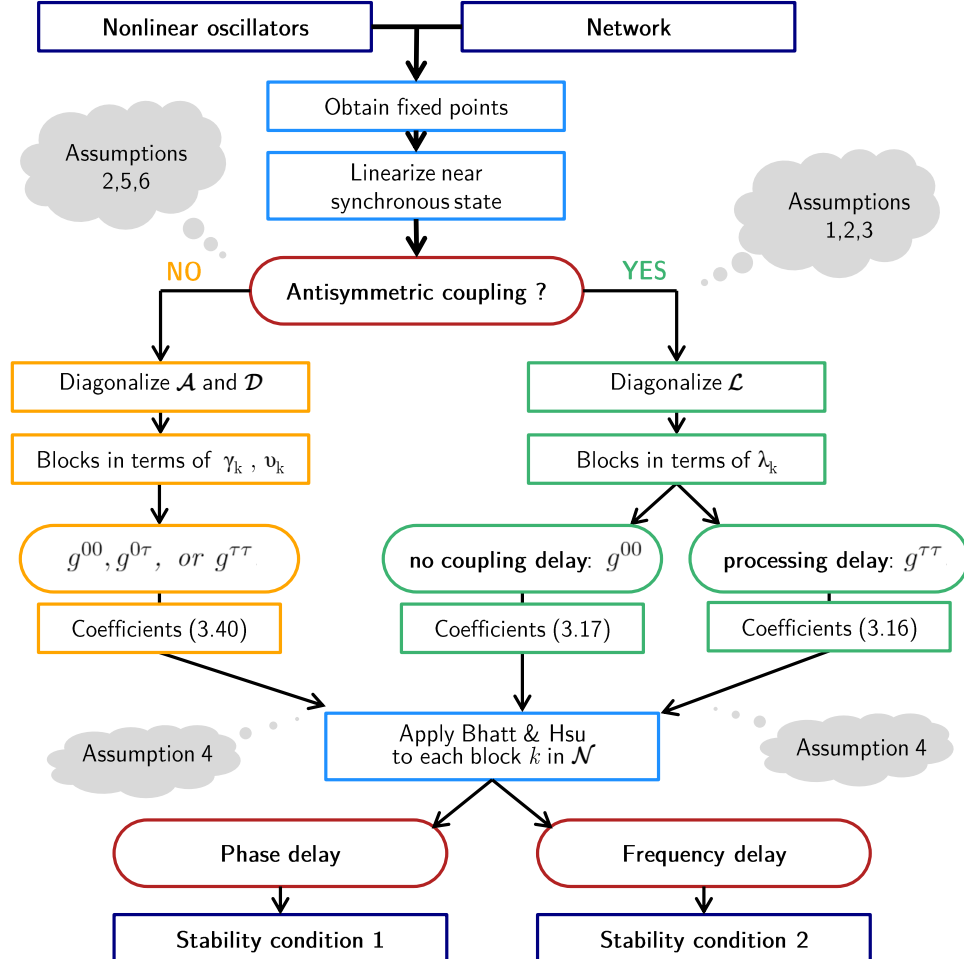


Figure 2: Flow chart of our delay master stability approach.

## 4. Power grids as dynamical networks

The power grid belongs to the most complex machines humans have built. Without doubt, it is the largest, extending from your multi socket at home to opposite ends of a continent. Our daily lives rely on its stable operation. In coming years, the ongoing transition towards renewable energies will substantially alter the structure and dynamical properties of the energy system. To understand how this affects power stability, we must look at the grid as a whole. Network theory provides the tools.

### 4.1. The power grid – today and tomorrow

Power grids [43, 44] fulfill the task of generating, transmitting, and distributing electrical energy while continuously balancing supply and demand. To accomplish this efficiently, conventional grids have been designed in multiple levels characterized by different voltages [45]. The extra high voltage (EHV,  $>110$  kV) transmission grid connects to large power plants (synchronous generators) and transports electricity over long distances [46]. Via transformer substations, the transmission grid is interfaced with a medium voltage distribution grid, which distributes power on smaller spatial scales. The mentioned multi socket at home plugs into the so-called low voltage ( $<1$  kV) distribution grid, which is linked by transformers to the medium voltage level.

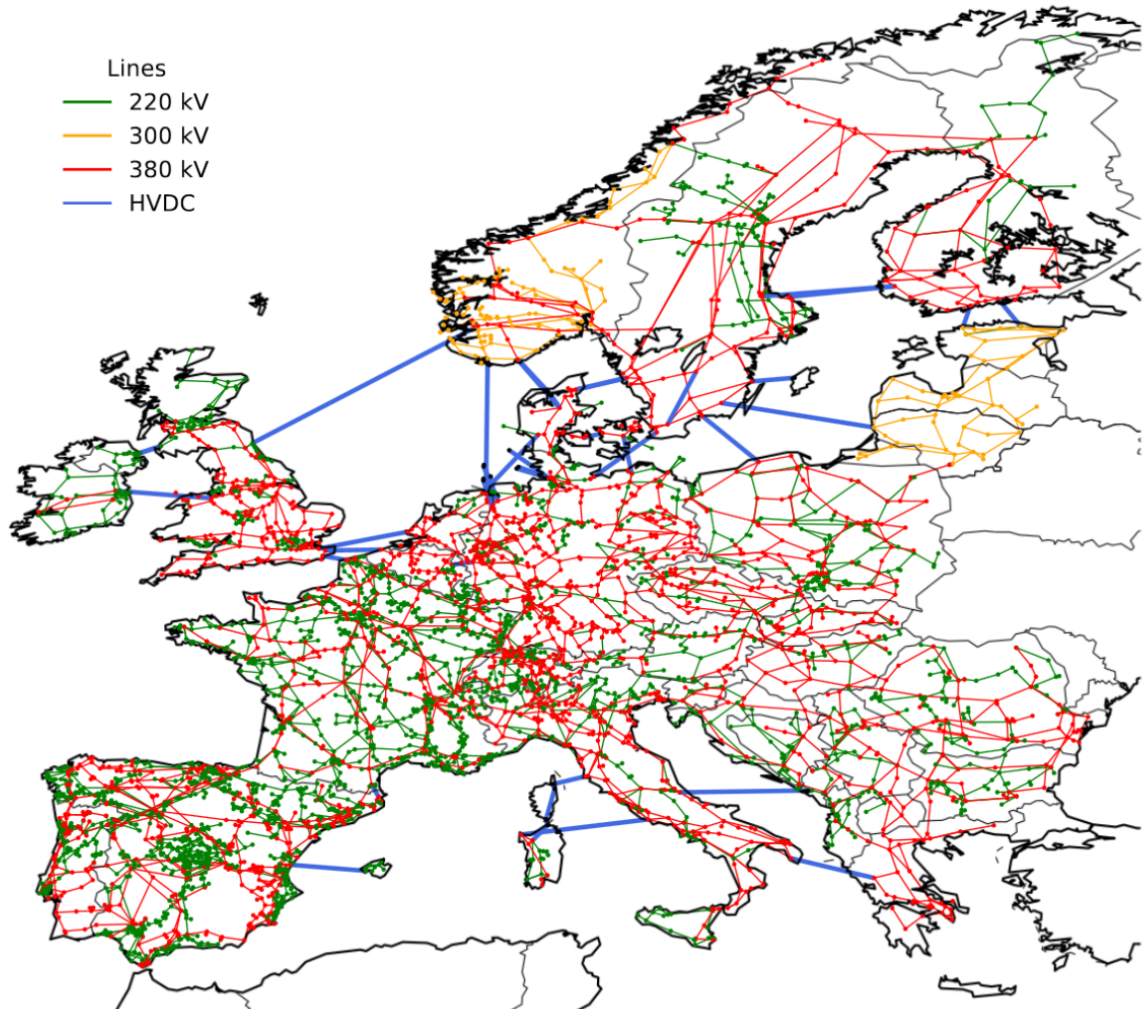


Figure 3: Europe's high voltage transmission grid (as of 2018, including elements under construction). The network model [42] contains 3657 nodes and 6001 edges. Stations and lines are colored based on their voltage level. Blue lines depict HVDC direct current highways. Image source: [42]

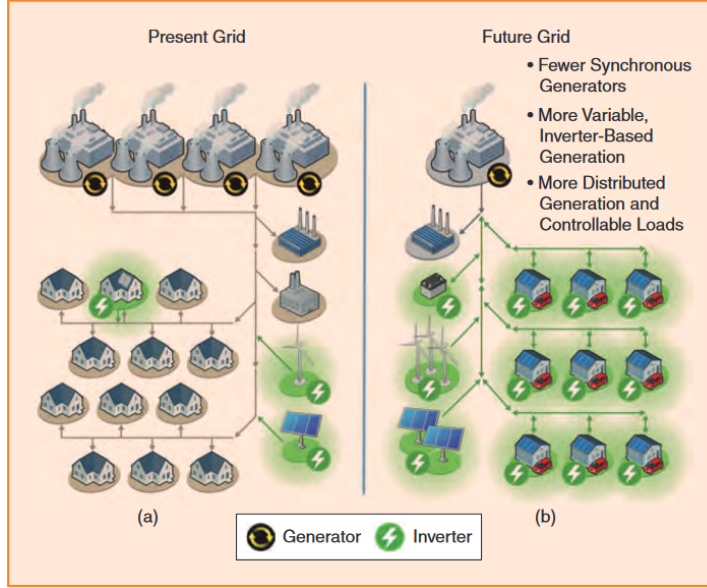


Figure 4: Schematic comparison of today's (a) and tomorrow's (b) power grid structure. Presently, electricity flows mainly from large, centralized synchronous generators to consumers. In the future grid, inverters will dominate, interfacing distributed renewable energy sources as well as prosumer units in a more meshed network. Adopted from [18]. (C) 2017 IEEE, used with permission.

Apart from high voltage direct current (HVDC) lines, the power grid runs with alternating current (AC). For stable operation it is critical that all generators, substations and consumption units synchronize with a nominal frequency of 50 Hz (or 60 Hz, in some parts of the world). Desynchronization, caused by an imbalance between supply and demand, could lead to cascading failures and wide-spread blackouts [47].

The hierarchical structure described above becomes increasingly inadequate to describe future power systems. While electricity used to flow mainly in one direction from large producers to consumers [18], the growing share of renewable energy sources [17, 21] induces a much more diverse generation landscape (see fig. 4). High-output power plants (synchronous generators powered by coal, gas, or nuclear fission) will be replaced by a large number of heterogeneously distributed renewable energy units, injecting power at all voltage levels [18]. As a consequence, the balancing of supply and demand will take place both locally and on the transmission level. With storage elements and solar-equipped homes, many dynamical actors in the grid become *prosumers* who sometimes produce and sometimes consume electricity [48]. Moreover, wind and solar power stations generate highly variable and uncertain output on timescales ranging from milliseconds to weeks [20, 21]. This demonstrates how both the topology and the dynamics of the power grid presently undergo a substantial change.

Synchronous generators like thermal power plants stabilize the power grid due to their inertia [49, 50]. Excess energy in the grid can be stored momentarily as rotational energy of the rotor, leading to a slight increase in frequency. Contrarily, if power production is below the desired set point, the rotor energy can compensate this for a moment by converting rotational to electrical energy. Thus, the system balances itself within a certain tolerance region. When distributed generators replace synchronous generators in future grids, the total inertia of the system is significantly reduced [50]. Power inverters which interface renewable generation units and prosumers to the grid are expected to take over the responsibility for synchronous stability. In other words, the safety and reliability of future power systems will depend eminently on the way the dynamics of so-called *grid-forming inverters* are controlled [18, 51]. However, the dynamical properties of synchronous machines and inverters are very different in principle [52]. It has been proposed to program the inverter control in a way that it mimics the behavior of synchronous generators by artificially adding inertia [53–55]. Other ideas suggest to regulate the

---

Weighted graph	$\leftrightarrow$	Power grid
Node	$\leftrightarrow$	Generation/consumption unit, inverter, transformer substation
Edge	$\leftrightarrow$	Power transmission line
Edge weight	$\leftrightarrow$	Line admittance

---

Table 1: Network interpretation of the power grid.

demand to deal with the volatile nature of solar and wind power production. [56]. For example, this could be achieved in a smart grid where all consumers regulate their consumption based on a varying energy price. These concepts motivate the power grid models analyzed in sections 5 and 6.

To fulfill the duty of stabilizing the grid, inverters must obviously monitor dynamical changes in the system. Measuring and processing this information inevitably takes time. This suggests that incorporating delays in power grid models becomes increasingly important. To date, the effect of delays on power system stability has not been fully studied [57].

## 4.2. A complex network perspective

The increasing complexity of the power grid suggests that we must consider the entire system as a whole. In other words, we expect the interactions between grid components to have a critical influence on the system's behavior.

Complex network theory provides a powerful foundation to study the power grid from a holistic and conceptual perspective. Without considering every detail of the real-world energy system, previous work has been able to draw significant conclusions about dynamical behavior and the effect of grid topology. For example, Hellmann et al. [58] recently uncovered that losses in transmission lines can lead to the desynchronization of single actors. Menck et al. [59] have shown how dead ends of power lines diminish stability. Such theoretical insight may serve as a point of reference for real-world implementation by grid designers and operators [60]. The survey [61] gives an overview of contributions that have studied power grids as complex networks.

Interpreting the power grid as a complex network seems rather intuitive (see tab. 1). Generally, nodes may represent power generation/consumption units or specifically the inverters that interface them to the grid, as well as storage elements and transformer substations between grid levels. Edges in the network naturally represent power transmission lines. Their weight is related to the maximal power they can transmit, which is given by the line admittance (see section 4.2.1). Complete information about the power grid structure is then stored in the network's adjacency matrix  $A$  or the corresponding Laplacian  $L$ .

However, a detailed model of the entire power grid would be too difficult to handle in most cases. Many studies therefore focus on a specific grid level (e.g. transmission grid [59], microgrid on distribution level [19]) or condense a group of similar units into one node (e.g. [56]). A model of the European high voltage transmission grid, illustrated in figure 3, gives an idea of the complexity of such a network. A different approach known as Kron reduction [62, 63] seeks to simplify the system by modeling loads as constant impedances and considering an effective network of generators [52].

What about the dynamics on the network? Due to the sinusoidal oscillation of the AC voltage (in steady-state operation), it is well established to model each node as a damped, driven inertial oscillator with natural frequency  $\Omega = 2\pi \cdot 50$  Hz [64]. Frequency stability then requires that all oscillators resynchronize with the common frequency  $\Omega$  after a perturbation. In the following, we derive the power flow equations and introduce the swing equation as a simple model to describe phase and frequency dynamics of the voltage in a power grid.

#### 4.2.1. Power flow

Consider the complex AC voltage  $V = U e^{i\theta}$  with amplitude  $U(t)$  and phase angle  $\theta(t)$ . The apparent power  $S$  is given as a product of voltage  $V$  and (complex conjugated) current  $\bar{I}$ ,

$$S := P + iQ = V\bar{I}, \quad (4.1)$$

where  $P$  and  $Q$  denote the active and reactive power, respectively [65]. A power grid consisting of  $N$  nodes is in steady-state operation when the power flow perfectly balances supply and demand. We can express this in the equation [58]

$$P_i^d = \sum_{j \neq i} P_{ij}, \quad i, j \in \bar{N}. \quad (4.2)$$

Here,  $P_i^d$  is the desired active power produced or consumed by the  $i$ -th node; it is positive for production and negative in the case of consumption. The right hand side represents the net power that flows away from node  $i$  to connected nodes  $j$ . The sum is negative when net power flows towards node  $i$ . Invoking Ohm's law, the current flowing through a transmission line from  $i$  to  $j$  reads

$$I_{ij} = \frac{V_i - V_j}{R_{ij} + iX_{ij}} = y_{ij}(V_i - V_j), \quad (4.3)$$

where the complex line admittance  $y_{ij}$ , as the reciprocal of the impedance  $Z_{ij} = R_{ij} + iX_{ij}$ , depends on the resistance  $R$  and reactance  $X$  of the power line [58]. We assume that  $y_{ii} = 0$  (neglecting shunt). Furthermore,  $y_{ij}$  is non-zero only if nodes  $i$  and  $j$  are connected. This illustrates the interpretation of line admittance as the weight of the edge  $i \leftrightarrow j$ . We introduce the nodal admittance matrix  $Y_{ij}$ , [56]

$$Y_{ij} := \begin{cases} -y_{ij} & i \neq j \\ \sum_{l \neq i} y_{il} & i = j \end{cases} \quad (4.4)$$

which resembles the Laplacian matrix of a weighted graph and thus contains complete information on the power grid structure. In electrodynamical terms, the real and imaginary parts of the admittance are labeled conductance  $G$  and susceptance  $B$ , respectively. We correspondingly define  $Y := G + iB$  in matrix notation. Using  $Y$ , the net outgoing currents  $I_i = \sum_j I_{ij}$  are compactly written as  $I = Y \cdot V$ , with nodal voltages  $V = (V_1, \dots, V_N)^\top$  and  $I = (I_1, \dots, I_N)^\top$  [58]. Then, the net outgoing power flow  $P_i^{el}$  at node  $i$  becomes

$$\begin{aligned} P_i^{el} &:= \sum_j P_{ij} \\ &= \operatorname{Re} \left( V_i \sum_j \bar{Y}_{ij} \bar{V}_j \right) \\ &= \operatorname{Re} \left( \sum_j U_i e^{i\theta_i} (G_{ij} - iB_{ij}) U_j e^{-i\theta_j} \right) \\ &= \operatorname{Re} \left( \sum_j U_i U_j (G_{ij} - iB_{ij}) [\cos(\theta_i - \theta_j) + i \sin(\theta_i - \theta_j)] \right). \end{aligned} \quad (4.5)$$

Let us simplify (4.5) for our purposes. In this thesis, we investigate the frequency stability of the grid voltage. Therefore, we set the amplitudes  $U_i$  to be constant and equal throughout the network [56, 66], i.e.  $U_i = U_0 \forall i$ . We furthermore assume a lossless grid, which implies  $Y_{ij} = iB_{ij} \forall i, j$ . Though power lines are not purely inductive in reality, inductive impedances

usually dominate over ohmic resistances, which motivates this approximation [52]. With  $G_{ij} = 0$  and homogenous amplitudes  $U_0$ , equation (4.5) yields<sup>9</sup>

$$P_i^{el} = \sum_j P_{ij} = \sum_j U_0^2 |B_{ij}| \sin(\theta_i - \theta_j) . \quad (4.6)$$

Combined with (4.2), equation (4.6) reveals the steady-state active power flow of a lossless power grid. In equilibrium, the magnitude of the power flow between nodes  $i$  and  $j$  depends on the phase angle difference  $\theta_i - \theta_j$  and on the quantity  $K_{ij} := U_0^2 |B_{ij}|$ . Physically, we may interpret  $K_{ij}$  as a coupling strength expressing the maximally transmittable power between nodes  $i$  and  $j$  [56]. As an odd function, the sine maintains antisymmetry: power flow from  $i$  to  $j$  equals negative power flow from  $j$  to  $i$  (we assume that  $|\theta_i - \theta_j| < \pi/2$ ).

#### 4.2.2. The swing equation

We have established above that the nodal phase angles  $\theta_i$  of the voltage determine power flows in the energy network (under the assumption of constant amplitudes). In equilibrium, the AC voltage oscillates synchronously with angular frequency  $\Omega$  at all nodes and the phase differences remain constant in time. Moving to a co-rotating reference frame (section 2.3), all  $\theta_i$  become constant, marking a synchronous fixed point.

To see how the phase angles evolve when the steady state is perturbed, we model each node as a damped, driven oscillator. Its phase dynamics are given by a second-order differential equation called the *swing equation*, [43, 56]

$$m_i \ddot{\theta}_i + \alpha_i \dot{\theta}_i = P_i^d - P_i^{el} . \quad (4.7)$$

Here,  $m_i$  denotes the moment of inertia and  $\alpha_i$  the damping constant of the  $i$ -th oscillator. As before,  $P_i^d$  denotes the power produced or consumed at node  $i$ , whereas  $P_i^{el}$  is the outgoing power flow. The swing equation 4.7 shows directly that the angular frequency deviation  $\omega_i = \dot{\theta}_i$  vanishes when the power flow balances supply and demand. If, say, more power is produced at node  $i$  than required by the network ( $P_i^d > P_i^{el}$ ), the frequency deviation  $\omega_i$  increases until the damping balances things out. Vice versa, under-production leads to a decrease in angular frequency.

Now, inserting (4.6) into the swing equation and slightly rearranging the result yields an inertial oscillator model governed by

$$m_i \ddot{\theta}_i = P_i^d - \alpha_i \dot{\theta}_i + \sum_j K_{ij} \sin(\theta_j - \theta_i) . \quad (4.8)$$

This is, in essence, a second-order Kuramoto model. The matrix  $K$  corresponds to the weighted adjacency matrix of the network.

In summary, we obtain a steady state of the power grid by solving the equilibrium power flow equations

$$0 = P_i + \sum_j K_{ij} \sin(\theta_j - \theta_i) . \quad (4.9)$$

Then, we can analyze the asymptotic stability of this steady state using model (4.8). But how does the presence of a delay affect stability in power grid models? This question will guide us through the following two sections. Note that there may be a phase delay in the coupling as well as a frequency delay in the local dynamics. We analyze both cases on the basis of concrete delay models proposed in the literature. Section 5 illuminates phase delays of droop-controlled inverters, while section 6 considers delayed frequencies in decentral smart grid control.

---

<sup>9</sup>Depending on the convention,  $B_{ij}$  may be negative for inductive lines. We take the absolute value to ensure positivity, such that power flows from nodes with larger phase angles to nodes with smaller phase angles.

## 5. Phase delay: Grid-forming inverters

We are now prepared to apply our delay master stability method to power grids. To study the case of phase delays, we consider the dynamical control of grid-forming inverters, which have been identified as a key concept of future renewable energy networks. Unlike synchronous generators, inverters do not feature an intrinsic relationship between frequency and power generation. One way to get around this is droop control, which programs the inverter to artificially create a linear dependence between frequency and active power [52, 67, 68]. Historically, droop control has found wide implementation in electrical engineering for power sharing between synchronous generators [69]. In a similar way, droop-controlled inverters equipped with a short-time energy storage can regulate their power output based on local angular frequency deviations; thus “forming” the grid. A major advantage is the decentrality of this scheme, as inverters require only local measurements of the frequency. This circumvents the need for a sophisticated communication system parallel to the grid. However, due to the measurement process and other technical details of the controller, the adjustment is assumed to carry a delay.

### 5.1. Droop-controlled inverter model with delay

Schiffer et al. [52] present a droop-controlled inverter model where the delay is represented by a low-pass filter. Here, we modify the original description and replace the filter by a constant delay  $\tau > 0$  (for details, see appendix A). We consider droop-controlled grid-forming inverters with phase and frequency dynamics governed by

$$\begin{aligned} \dot{\phi}_i &= \omega_i \\ m_i \dot{\omega}_i &= -\alpha_i \omega_i + \beta_i (P_i^d - P_i(\phi^\tau)) . \end{aligned} \quad (5.1)$$

Here,  $m_i > 0$  and  $\alpha_i > 0$  are inertias and damping constants, respectively;  $\beta_i > 0$  denotes the droop constant of the  $i$ -th oscillator,  $P_i^d$  represents the desired active power set points and the delayed function  $P_i(\phi^\tau)$  is given by

$$P_i(\phi^\tau) = - \sum_{j=1}^N K_{ij} \sin(\phi_j(t - \tau) - \phi_i(t - \tau)) , \quad (5.2)$$

where  $K_{ij} = U_0^2 B_{ij}$  is the weighted adjacency matrix of the network. The dynamical variables  $\phi_i$  and  $\omega_i$  are expressed in coordinates of a co-rotating reference frame as usual; the voltage amplitude is assumed to be time-independent.

### 5.2. Delay master stability analysis

Let us apply the delay master stability approach derived in section 3 to investigate the linear stability of model (5.1). We will follow the procedure step by step to illustrate our method by means of a concrete example.

We are dealing with a coupling processing delay in the phase, where  $f^\tau = g^{00} = g^{0\tau} = 0$ . Thus, (5.1) is composed of the functions  $f_i^0$  and  $g^{\tau\tau}$ :

$$f_i^0(x_i) = \begin{pmatrix} \omega_i \\ -\frac{\alpha_i}{m_i} \omega_i + \frac{\beta_i}{m_i} P_i^d \end{pmatrix} , \quad g^{\tau\tau}(x_i) = \begin{pmatrix} 0 \\ \frac{\beta_i}{m_i} \sin(\phi_j^\tau - \phi_i^\tau) \end{pmatrix} . \quad (5.3)$$

Performing the linearization, the corresponding Jacobians read

$$D_i f^0 = \begin{bmatrix} 0 & 1 \\ 0 & -\frac{\alpha_i}{m_i} \end{bmatrix} , \quad D_{ij}^{1/2} g^{\tau\tau} = \mp \cos(\phi_j^* - \phi_i^*) \begin{bmatrix} 0 & 0 \\ \frac{\beta_i}{m_i} & 0 \end{bmatrix} \quad (5.4)$$

Equation (5.4) shows directly that the model fulfills assumption 1 (antisymmetric coupling), i.e.  $D_{ij}^1 g^{\tau\tau} = -D_{ij}^2 g^{\tau\tau}$ . Assumption 4 (no coexistence of phase and frequency delay) is also satisfied because we have a phase delay only. To satisfy assumptions 2 and 3 (which we need in order to write Kronecker products), we must require

$$\frac{\alpha_i}{m_i} = \tilde{\alpha} \quad \text{and} \quad \frac{\beta_i}{m_i} = \tilde{\beta} \quad \forall i \quad \Rightarrow \quad \alpha_i = \frac{\tilde{\alpha}}{\tilde{\beta}} \beta_i \quad \forall i . \quad (5.5)$$

Note that only the *ratios* of damping and inertia – as well as droop gain and inertia – must be identical for all nodes. In a sense, this means that assumptions 2 and 3 are slightly more general than allowing only strictly identical oscillators. For example, moments of inertia may be different from oscillator to oscillator, as long as the droop and damping constants are modeled to meet the above condition. As demanded by assumption 3, we can separate  $D_{ij}^2 g^{\tau\tau}$  into a node-dependent factor  $w_{ij} := \cos(\phi_j^* - \phi_i^*)$  and a global Jacobian  $G^{\tau\tau}$ . Together with  $D_i f^0 = F^0$  for all  $i$ , we find

$$F^0 = \begin{bmatrix} 0 & 1 \\ 0 & -\tilde{\alpha} \end{bmatrix}, \quad G^{\tau\tau} = \begin{bmatrix} 0 & 0 \\ \tilde{\beta} & 0 \end{bmatrix}. \quad (5.6)$$

The effective adjacency matrix  $\mathcal{A}_{ij}$  is thus given by  $\mathcal{A}_{ij} = K_{ij} \cos(\phi_j^* - \phi_i^*)$ . To ensure that  $\mathcal{A}$  has no negative entries, we restrict the steady state angular differences to  $|\phi_j^* - \phi_i^*| < \pi/2$  for all  $i, j$ . This leads to the effective Laplacian matrix  $\mathcal{L}$ ,

$$\mathcal{L}_{ij} = \begin{cases} -K_{ij} \cos(\phi_j^* - \phi_i^*) & i \neq j \\ \sum_{l \neq i} K_{lj} \cos(\phi_l^* - \phi_i^*) & i = j \end{cases}, \quad (5.7)$$

which we need to diagonalize. In terms of the eigenvalues  $\lambda_i$  of  $\mathcal{L}$ , we arrive at the  $2 \times 2$  block equation

$$\begin{pmatrix} \dot{\theta}_k \\ \dot{\varpi}_k \end{pmatrix} = \begin{bmatrix} 0 & 1 \\ 0 & -\tilde{\alpha} \end{bmatrix} \begin{pmatrix} \theta_k \\ \varpi_k \end{pmatrix} - \lambda_k \begin{bmatrix} 0 & 0 \\ \tilde{\beta} & 0 \end{bmatrix} \begin{pmatrix} \theta_k^\tau \\ \varpi_k^\tau \end{pmatrix}, \quad (5.8)$$

where  $\theta_k$  and  $\varpi_k$  denote the phase angles and angular frequency deviations in the eigenspace of  $\mathcal{L}$ , respectively. In second-order DDE form, a block (5.8) reads

$$\ddot{\theta}_k = -\tilde{\alpha}\dot{\theta}_k - \tilde{\beta}\lambda_k\theta_k^\tau. \quad (5.9)$$

Equation (5.9) is a special case of (3.15) and thus compatible with the Bhatt-Hsu stability analysis. As coefficients (3.16), we have

$$a_k = \tilde{\alpha}, \quad b_k = 0, \quad s_{1,k} = 0, \quad s_{0,k} = \lambda_k \tilde{\beta}.$$

Before we can make use of Bhatt and Hsu's theorem 1, we must find the wanted root  $y_1$  of the imaginary part  $\mathcal{G}(y)$  of the characteristic function. Since  $\mathcal{G}(y) = -y^2 \sin y + \tilde{\alpha}\tau y \cos y$  is independent of  $\lambda_k$ , we only have to do this once, and the root is uniquely determined in terms of  $\tilde{\alpha}$  and  $\tau$  by the implicit equation

$$y_1 = \tilde{\alpha}\tau \cot(y_1), \quad y_1 \in (0, \pi]. \quad (5.10)$$

The delay dependence of (5.10) is plotted in figure 5. Now, stability condition 1 states that a synchronous state of the model is stable if and only if

$$0 < \lambda_k \tilde{\beta} < \frac{1}{\tau^2} \sqrt{y_1^4 + (\tilde{\alpha}\tau y_1)^2} \quad \forall k \in \{2, \dots, N\}. \quad (5.11)$$

Note that the transversal set  $\mathcal{N}$  (definition 3) excludes  $k = 1$  because there is no local delay. The left inequality in (5.11) does not restrict anything because every Laplacian matrix (of a

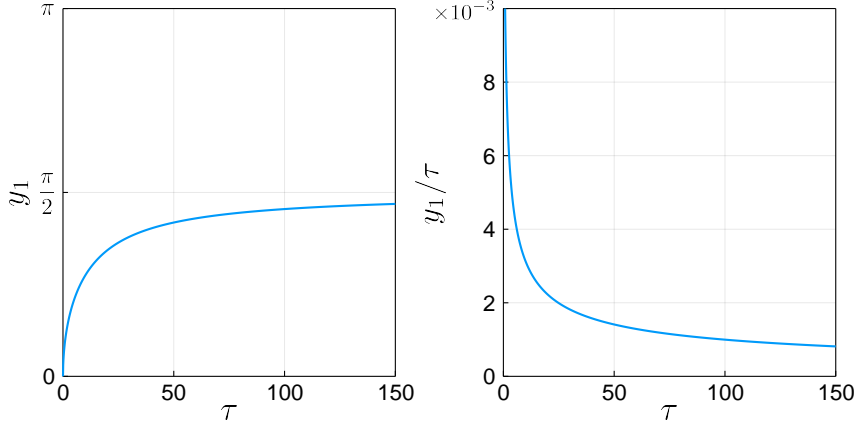


**Figure 5: Delay-dependence of the root  $y_1$ .** Left: The plot shows that the root  $y_1$  located in the interval  $(0, \pi]$  monotonically approaches  $\pi/2$  as  $\tau \rightarrow \infty$ . Right: Dividing  $y_1$  by  $\tau$  reveals that the fraction decreases monotonically with increasing delay. This implies the existence of precisely one critical delay  $\tau_c$ .

connected graph) has the property that  $\lambda_k > 0$  for all  $k \geq 2$ . Since  $\tilde{\beta} > 0$ , the right inequality holds for all  $\lambda_k$  whenever it is satisfied by the largest eigenvalue  $\lambda_N$  (see section 3.2.3). This reduces the set of constraints to a single criterion, delivering the delay master stability condition we were looking for:

$$\boxed{\lambda_N < \frac{1}{\tilde{\beta}} \sqrt{\left(\frac{y_1}{\tau}\right)^4 + \tilde{\alpha}^2 \left(\frac{y_1}{\tau}\right)^2}} \quad (5.12)$$

Thus, we have succeeded in contrasting information on the network structure, encoded in the maximum Laplacian eigenvalue  $\lambda_N$ , with dynamical information determined by  $\tilde{\alpha}, \tilde{\beta}$ , and  $\tau$ . We may write the associated delay master stability function as

$$\sigma(\lambda_N, \tau) = \lambda_N - \frac{1}{\tilde{\beta}} \sqrt{\left(\frac{y_1}{\tau}\right)^4 + \tilde{\alpha}^2 \left(\frac{y_1}{\tau}\right)^2}. \quad (5.13)$$

In regions where the combination of  $\lambda_N$  and  $\tau$  yields  $\sigma < 0$ , the fixed point is linearly asymptotically stable. As figure 5 reveals, the fraction  $y_1/\tau$  – and thus the entire square root in (5.12) – decreases monotonically with increasing delay. For fixed  $\tilde{\alpha}$  and  $\tilde{\beta}$ , this implies that the stable range for  $\lambda_N$  shrinks to zero as  $\tau \rightarrow \infty$ . In fact, for any model (5.1) fulfilling (5.5) there exists precisely one critical delay

$$\tau_c = \tau_c(\tilde{\alpha}, \tilde{\beta}, \lambda_N).$$

A synchronous state that is linearly stable without delay is also linearly stable for all  $\tau < \tau_c$ , whereas it is unstable for all  $\tau \geq \tau_c$ . The critical delay may be increased by lowering the rescaled droop gain  $\tilde{\beta}$  or raising the rescaled damping  $\tilde{\alpha}$ . Furthermore, in the case of homogenous coupling, weaker coupling leads to a smaller  $\lambda_N$  and therefore enhances delay stability.

In the following, we test our delay master stability condition on two simple network topologies.

### 5.3. Four-node star network

Let us begin with an elementary building block of a power grid: a star. Certainly, this choice does not live up to the strongly meshed topologies of inverter-based energy systems. Nonetheless, in the vicinity of a generation unit, a star topology may qualify as a local approximation. It serves as a basic starting point and will allow us to compare results with our analysis of frequency delays in section 6.

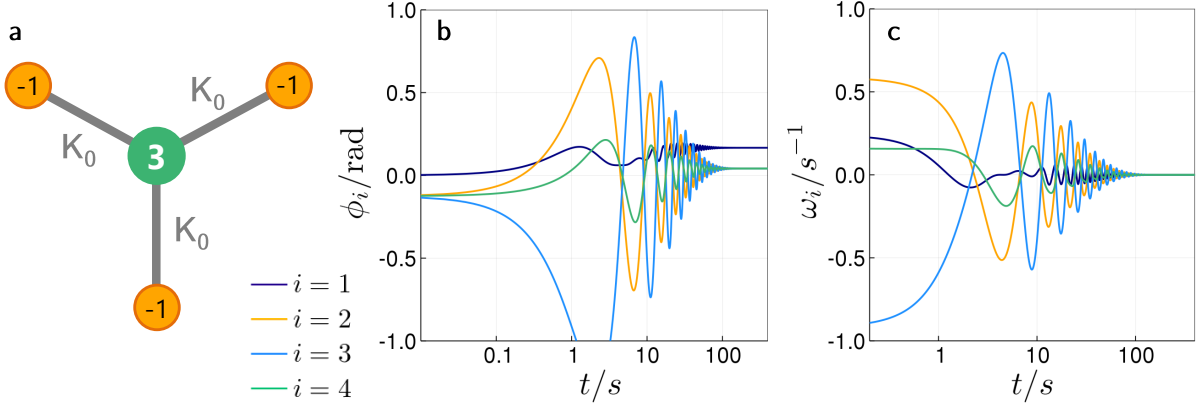


Figure 6: **Undelayed dynamics on the star topology.** (a) Illustration of the four-node star network. A producer in the middle generating the power  $P_1 = 3P_0$  supplies three consumers with  $P_{2,3,4} = -P_0$ . All lines have equal admittance  $K_0$ . (b-c) Simulation of phase and angular frequency dynamics after a small perturbation of the nodal frequencies without delay ( $\tau = 0$ ). The perturbations have been chosen randomly from the interval  $[-0.4\pi, 0.4\pi]$ , which corresponds to the frequency tolerance range in power grids of  $50 \pm 0.2$  Hz. After  $\approx 100$ s, the frequencies (c) re-synchronize and phase angles (b) reestablish the equilibrium phase difference  $\Delta\phi^* = \arcsin(P_0/K_0)$ . Thus, the fixed point is stable without delay. Parameter values are  $P_0 = 1 \text{ s}^{-2}$ ,  $K_0 = 8 \text{ s}^{-2}$ ,  $\tilde{\alpha} = 0.1 \text{ s}^{-1}$ , and  $\tilde{\beta} = 0.07$ . Time is plotted on a log2 scale.

We consider a four-node star network with one generation unit in the center and three identical consumers around it, connected to the generation unit by transmission lines with equal capacity  $K_0$ . (see figure 6a). The weighted adjacency matrix of this configuration is

$$K = \begin{bmatrix} 0 & K_0 & K_0 & K_0 \\ K_0 & 0 & 0 & 0 \\ K_0 & 0 & 0 & 0 \\ K_0 & 0 & 0 & 0 \end{bmatrix}. \quad (5.14)$$

All actors are interfaced via droop-controlled inverters. In steady-state operation, the generator injects the power  $P_+ = 3P_0$ , while each consumer uses  $P_- = -P_0$  such that the total net power balance is zero:

$$\sum_{i=1}^4 P_i = 0, \quad (5.15)$$

with  $P_1 = P_+$  and  $P_{2,3,4} = P_-$ . The inverters are modeled with identical damping constants  $\alpha$ , droop gains  $\beta$ , and moments of inertia  $m$  according to (5.1). Exploiting the symmetry of the star, a synchronous fixed point  $\Delta\phi^*$  (all units run with angular frequency  $\Omega$ ) is defined by the equilibrium power flow equation,

$$0 = P_0 - K_0 \sin(\Delta\phi^*), \quad (5.16)$$

where  $\Delta\phi^* = \phi_+^* - \phi_-^*$  denotes the phase difference between the producer and any of the consumers. (The choice of a co-rotating coordinate system grants us one degree of freedom for the phase angles.) In this simple, symmetric case, we find the analytic solution

$$\Delta\phi^* = \arcsin\left(\frac{P_0}{K_0}\right). \quad (5.17)$$

Since the inverse sine is restricted to the domain  $[-1, 1]$ , a fixed point only exists if  $P_0 \leq K_0$ , which fits to the intuition that the power production or consumption cannot exceed the maximally transmittable power through the adjacent lines.

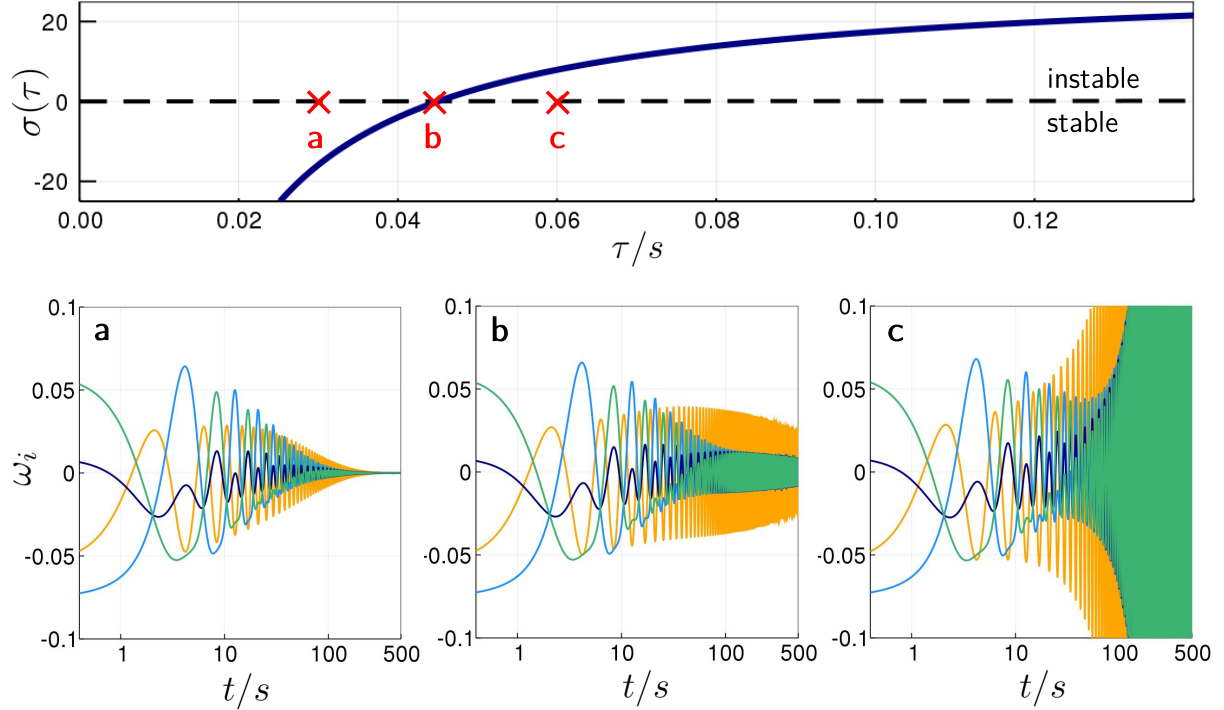


**Figure 7: Dynamics near the critical delay.** Top: Delay master stability function  $\sigma(\lambda_N, \tau)$  of the star grid inverter model as a function of  $\tau$ . The synchronous state is stable if and only if  $\sigma < 0$ . We see that the system starts out stable for small delays and passes a critical point after roughly 45ms. Parameter values for the plot are  $P_0 = 1 \text{ s}^{-2}$ ,  $K_0 = 8 \text{ s}^{-2}$ ,  $\tilde{\alpha} = 0.1 \text{ s}^{-1}$ , and  $\tilde{\beta} = 0.07 \text{ s}^{-1}$ . This yields  $\lambda_N \approx 31.75$  and  $\tau_c \approx 45\text{ms}$ . Bottom: We verify our result with simulations for three different delays near criticality:  $\tau_a = 30\text{ms}$ ,  $\tau_b = 44\text{ms}$ ,  $\tau_c = 60\text{ms}$ . As expected, (a) and (b) are stable, (c) is not. Close to  $\tau_c$  (b), the system converges much slower than at (a). The three plots show the frequency deviations  $\omega_i$  after a random perturbation on a log2 time scale.

To calculate something, we need numbers. Typical values in the power grid modeling literature are  $P_0 = 1 \text{ s}^{-2}$ ,  $K_0 = 8 \text{ s}^{-2}$ , and  $\tilde{\alpha} = 0.1 \text{ s}^{-1}$  [48, 59]. We choose a droop constant of  $\tilde{\beta} = 0.07$  in order to obtain similar proportions between power set point and droop gain as in [52]. From (5.14) and (5.17) we construct the Laplacian matrix, which we diagonalize numerically using the `LinearAlgebra.jl` package [70] of the Julia programming language ( $\lambda_N \approx 31.75$ ). For our delay master stability analysis, we furthermore need the root  $y_1$ , which we compute using Julia's `Roots.jl` package [71].

**Critical delay.** Figure 6 (b-c) shows a simulation of the system's transient behavior after a small random perturbation in the absence of a delay ( $\tau = 0$ ). We find that with the chosen parameter values, the synchronous state is stable without delay. Assured of this, we calculate the delay master stability function for delays up to 0.15 s. The result is depicted in figure 7. According to our delay stability method, the transition from stability to instability occurs at  $\tau_c = 45 \text{ ms}$ . For verification, we run simulations near criticality using the DDE functionality of `DifferentialEquations.jl` [72] with the `Tsit5` solver algorithm (see figure 7). As a history function we specify a constant random perturbation of all four nodal frequencies. Theory and experiment confirm each other: as predicted by the delay master stability condition, the system does not return to the synchronous 50 Hz state for delays larger than the critical delay  $\tau_c = 45 \text{ ms}$ .

**Influence of isolated dynamics.** Seeing that our method succeeds, we want to analyze how the isolated dynamics of the oscillators affect stability. We compute the delay master stability function  $\sigma$  for a variety of different parameter combinations, assuming that they are identical for

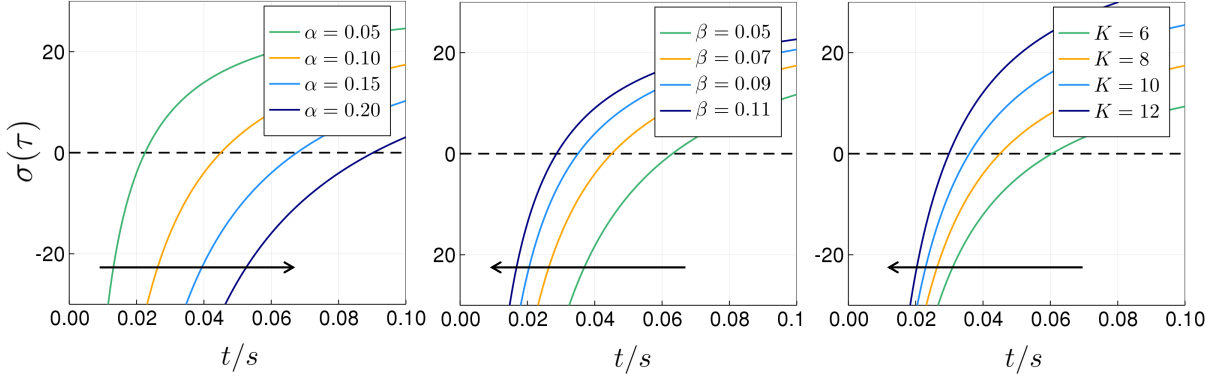


Figure 8: **Critical delay as a function of dynamical parameters.** All plots show delay master stability functions  $\sigma(\tau)$  for various parameter combinations. Left: The damping  $\tilde{\alpha}$  is varied from  $0.05 \text{ s}^{-1}$  to  $0.2 \text{ s}^{-1}$ . Center:  $\sigma(\tau)$  as a function of the droop constant  $\tilde{\beta}$  in a range from 0.05 to 0.11. Right: Different coupling strengths  $K_0$  between 6 and  $12 \text{ s}^{-2}$ . Parameter values not explicitly given are always  $P_0 = 1 \text{ s}^{-2}$ ,  $K_0 = 8 \text{ s}^{-2}$ ,  $\tilde{\alpha} = 0.1 \text{ s}^{-1}$ , and  $\tilde{\beta} = 0.07$ . The black arrows indicate whether the critical delay  $\tau_c$  (given by  $\sigma = 0$ ) increases or decreases as the respective dynamical variable is increased.

all nodes. A selection of results is displayed in figure 8. In summary, stronger damping prolongs the *window of stability*  $[0, \tau_c]$ , while an increase in the droop gain  $\tilde{\beta}$  or the coupling strength  $K$  decreases the critical delay. This seems physically reasonable – strong damping will make the system more resilient to perturbations, and reducing the droop gain essentially diminishes the influence of the delayed control. Since the delay appears in the coupling term, a weaker coupling strength also weakens the impact of the delay.

## 5.4. Small-world networks

The four-node star topology allowed us to field-test our delay master stability method and gain some insight into how *dynamical* parameters influence the stability of a delay system. Now, let us take our analysis to the next level. To see how delay stability depends on the network *structure*, we study a class of networks which comes somewhat closer to the complexity of actual power grids.

In 1998, Watts and Strogatz developed a network model which exhibits *small-world* characteristics [73]; that is, they feature relatively high clustering as well as small characteristic path lengths. The motivation behind this was that many real-world networks are too heterogeneous to be described by regular lattices, yet too ordered to qualify as purely random. Watts-Strogatz small-world networks conquer the space in between those two extremes by randomly rewiring edges of a regular graph. Starting out with a ring of  $N$  nodes, each having equal (even) degree

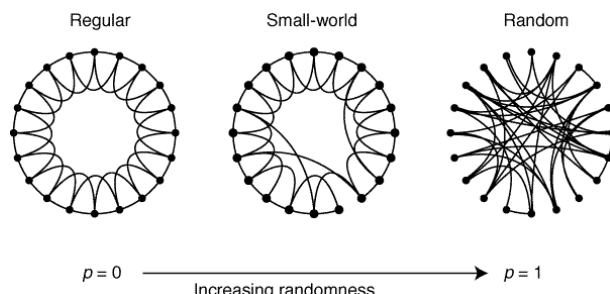
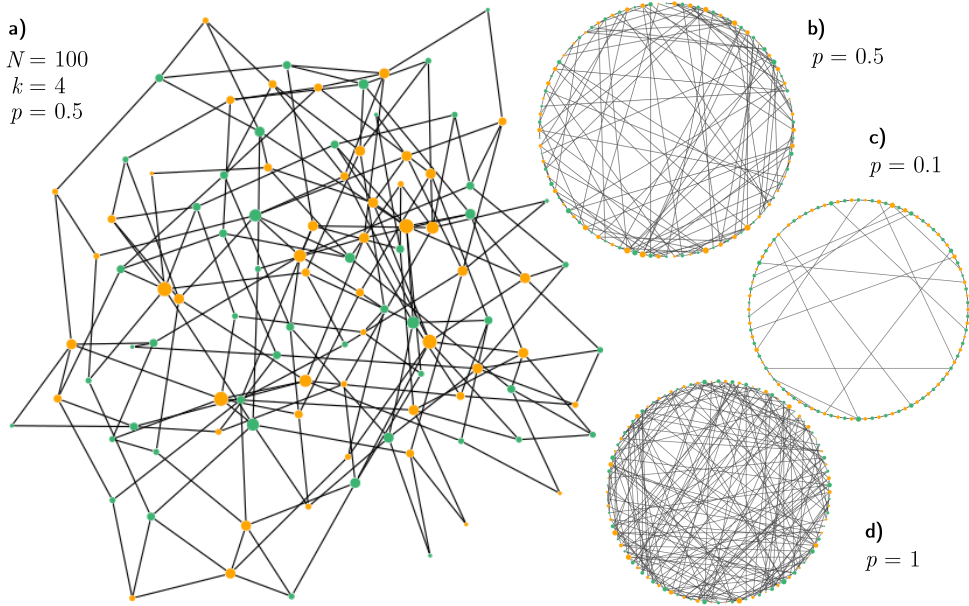


Figure 9: **The Watts-Strogatz network model.** Random rewiring of edges allows to interpolate between completely regular and totally random graphs. Small-world networks lie somewhere in between. Source: [73], used with permission.



**Figure 10: Watts-Strogatz power grids.** We consider networks of 50 producers (green), 50 consumers (orange), and a total of 200 transmission lines. The figure shows three different realizations of Watts-Strogatz networks with different randomness  $p$ . (a) and (b) are plots of the same graph in spring and circular layout, respectively. (c) and (d) illustrate the largely different topology of almost regular and fully random networks. The graphs are generated and plotted in Julia using LightGraphs and GraphPlot [76, 77].

$k$ , the rewiring process reconnects each edge with probability  $p$ . Interpolating  $p$  between zero and one, we obtain different degrees of disorder from completely regular to totally random (see figure 9). This versatility, tunable by three parameters  $N, p, k$ , allowed the model to become extremely popular in various fields of science.

Many real-world dynamical systems reveal small-world characteristics, including social networks [14], the neural network of *Caenorhabditis elegans* [73], protein-protein interactions [74], and the power grid of the Western United States [73, 75]. Whether power grids are generally small-world networks is answered controversially in the literature [61]. Nonetheless, we may expect inverter-based power grids to lie somewhere within the limits of pure randomness and regularity.

Several publications on the network structure of power grids [59–61] mention average degrees of  $k \approx 2 \sim 3$ . We argue that future inverter-based grids, especially in microgrids on distribution level, may be more densely meshed. Therefore, we choose a degree of  $k = 4$ . In the following, we construct the initial ring of the Watts-Strogatz graph by alternating consumers with power usage  $P_- = -P_0$  and generators producing  $P_+ = P_0$  each. Like this, we have  $N/2$  producers,  $N/2$  consumers, and in power flow equilibrium  $\sum_i P_i = 0$ ,  $i \in \bar{N}$ .

**Irregularity narrows the window of stability.** First, we set  $N = 100, k = 4$  to examine the stability as a function of the rewiring probability  $p$ . To generate Watts-Strogatz networks we utilize the LightGraphs.jl package [76] in Julia. Figure 10 illustrates a few realizations of such graphs. In the case  $p = 0$ , the network is completely regular, and each generator is linked directly to its two neighboring consumers. Note that the remaining edges connect generators to consumers and consumers to consumers, respectively. Since in the steady-state there exist only two phase angles,  $\phi_+^*$  for all producers and  $\phi_-^*$  for all consumers, line admittances between nodes of equal type become virtually zero in equilibrium. As soon as a perturbation arises, however, those links generally have non-zero admittance.

Networks with  $p > 0$  do not feature this symmetry because of the random rewiring of edges. We compute the critical delay  $\tau_c(p)$  as a function of  $p$  in steps of length 0.1. To account for the

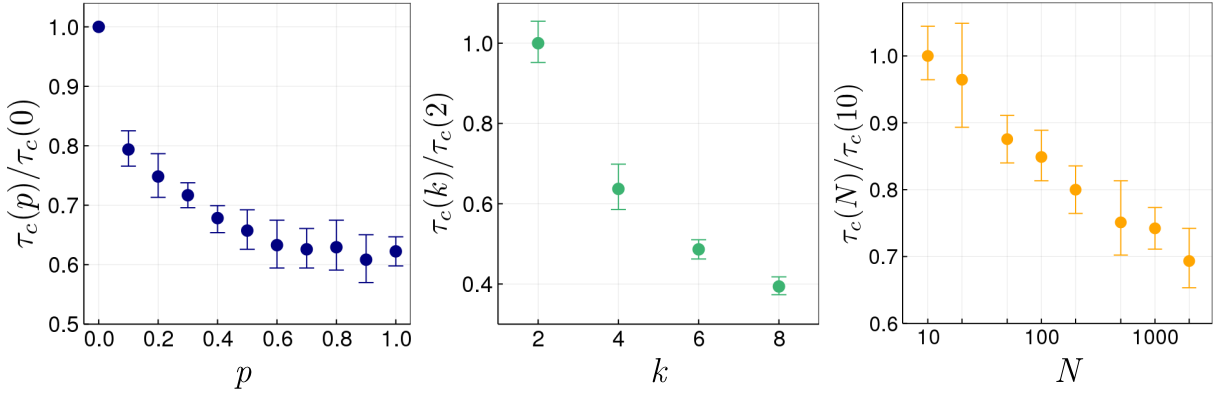


Figure 11: **Critical delay in Watts-Strogatz networks.** The three plots show how the critical delay  $\tau_c$  changes as a function of the three Watts-Strogatz model parameters  $p$ ,  $k$ , and  $N$ . Left: Rewiring probability  $p$  varied from 0 to 1. Center: Average degree  $k$  in a range from 2 to 8. Right: Varying the system size  $N$  from 10 to 2000 on a log10 scale. Vertical axes are normalized to the maximum value of data points. The error bars indicate the standard deviation arising from averaging over 10 network realizations each. Parameter values not explicitly given are  $N = 100$ ,  $k = 4$ ,  $p = 0.5$  as well as  $P_0 = 1 \text{ s}^{-2}$ ,  $K_0 = 8 \text{ s}^{-2}$ ,  $\tilde{\alpha} = 0.1 \text{ s}^{-1}$ , and  $\tilde{\beta} = 0.07$ .

stochastic behavior of the Watts-Strogatz model, we average over 10 network realizations for each  $p$ . The results are presented in figure 11. It shows that  $\tau_c$  is maximal for completely regular graphs ( $\tau_c(0) \approx 28$  ms). The rewiring of links narrows the window of stability by roughly 15 to 45%. Though there seems to be a trend of decreasing critical delay for increasing randomness, the stochastic uncertainty of samples from an ensemble of graphs makes it difficult to deduct more detailed information without further analysis.

**More cables don't help.** In this step, we set  $N = 100$ ,  $p = 0.5$  and vary the degree  $k$ . Since the Watts-Strogatz model allows only even mean degrees, we limit the set to  $k = 2, 4, 6, 8$ . As before, we average over ten samples each. The corresponding mean critical delays are shown in the center plot of figure 11. Interestingly, more links between nodes seem to impair the stability with delay. For  $k = 6$ , the window of stability is just about half of the stable regime for  $k = 2$ .

**Large networks diminish delay stability.** The last knob left to turn is the system size  $N$ . We consider networks with 10, 20, 50, 100, 200, 500, 1000, and 2000 nodes<sup>10</sup>. Again, we compute the critical delay, averaging each network size over ten realizations. The results are presented in the right plot of figure 11. As can be seen,  $\tau_c$  is largest for  $N = 10$  and decreases with increasing system size. The decrease appears to be roughly exponential because the data points show an approximately linear decay on a log10 scale  $N$  axis.

Generally, it seems that the more complex the network gets the shorter the delay has to be to maintain synchronous stability.

<sup>10</sup>Congratulations to my faithful computer, who tackled the  $2000 \times 2000$  matrix in just under 13 hours!

## 6. Frequency delay: Decentral smart grid control

Let us complete the picture by considering a system in which a frequency delay occurs. As a concrete example, we adopt a model proposed by Schäfer et al. [48, 56] as a decentral control scheme for smart grids. While many smart grid concepts involve extensive communication between a central control center and all consumption units, the notion of decentral smart grid control makes use of the frequency as a locally available parameter. As mentioned before, the angular frequency deviation of a node is positive when there is excess energy in the network and negative in the case of underproduction. Basically, this is all the information needed to control individual production or consumption. The idea is now to relate the current energy price to the angular frequency deviation: if the frequency increases, indicating excess energy, the price drops to motivate more consumption. Reversely, for negative frequency deviations the price is high to stimulate reduced energy usage. Realizing this control scheme requires continuous frequency measurements and, based on this data, the calculation of the current energy price. Schäfer et al. postulate that this induces a delayed reaction, causing a frequency delay.

### 6.1. A delayed demand response model

The model proposed in [48] (without averaging, see the reference) is a system of  $N$  oscillators governed by

$$\ddot{\phi}_i = P_i - \alpha \dot{\phi}_i + \sum_j K_{ij} \sin(\phi_j - \phi_i) - \gamma \dot{\phi}_i(t - \tau), \quad (6.1)$$

where  $P_i$  is the produced/consumed power at node  $i$ ,  $\alpha > 0$  and  $K = (K_{ij})$  denotes the usual weighted adjacency matrix. The final term with the delay  $\tau$  represents a linear price-frequency relation, which is tuneable through the *price elasticity*  $\gamma > 0$ . It acts as a second, delayed damping term.

### 6.2. Delay master stability analysis

We now derive stability conditions for model (6.1) using our delay master stability method. Many steps are similar to the procedure outlined in section 5.2. For this reason, we present a shorter version here and point to section 5.2 for a more detailed example.

The model has delayed and undelayed isolated dynamics  $f^0$  and  $f^\tau$ , while the coupling term is purely instantaneous ( $g^{00}$ ). Fixed points are determined as solutions to the set of equations

$$0 = P_i + \sum_j K_{ij} \sin(\phi_j - \phi_i). \quad (6.2)$$

In the linearized system, the Jacobians read

$$Df^0 = \begin{bmatrix} 0 & 1 \\ 0 & -\alpha \end{bmatrix}, \quad Df^\tau = \begin{bmatrix} 0 & 0 \\ 0 & -\beta \end{bmatrix}, \quad D_{ij}^{1/2} g^{00} = \mp \cos(\phi_j^* - \phi_i^*) \begin{bmatrix} 0 & 0 \\ 1 & 0 \end{bmatrix}. \quad (6.3)$$

Since the Jacobians of the isolated functions  $F^0 = Df^0$  and  $F^\tau = Df^\tau$  are identical for all nodes, the system immediately satisfies assumption 2. Furthermore, assumption 3 is fulfilled by absorbing the term  $\cos(\phi_j^* - \phi_i^*)$  into the effective adjacency matrix  $\mathcal{A}$ . Assumptions 1 (antisymmetric coupling) and 4 (single delay term) also hold, as is easily checked.

Projected in the eigenspace of the effective Laplacian  $\mathcal{L}$  (5.7), the linearized system is given by

$$\ddot{\theta}_k = -\alpha \dot{\theta}_k + \lambda_k \theta_k - \gamma \dot{\theta}_k^\tau, \quad (6.4)$$

where the set of  $\lambda_k$  denotes the eigenvalues of  $\mathcal{L}$ . Comparing this expression with (3.15), the coefficients in (3.17) become

$$a_k = \alpha, \quad b_k = \lambda_k, \quad s_{1,k} = \gamma, \quad s_{0,k} = 0.$$

The stability of a fixed point solution of model (6.1) is determined by stability condition 2 (3.34). Since  $\gamma > 0$ , the fixed point is stable if and only if

$$\boxed{\gamma\tau < \frac{1}{y_k^*} \sqrt{(y_k^{*2} - \lambda_k\tau^2)^2 + (\alpha\tau y_k^*)^2}} \quad (6.5)$$

We can write this condition as a delay master stability function,

$$\sigma(\lambda, \tau) = 1 - \frac{1}{\gamma\tau y^*(\lambda, \tau)} \sqrt{(y^*(\lambda, \tau)^2 - \lambda\tau^2)^2 + (\alpha\tau y^*(\lambda, \tau))^2}. \quad (6.6)$$

For stability it is necessary and sufficient that, given a certain  $\tau$ , all  $\lambda_k$  lie in regions where  $\sigma < 0$ . By writing  $y_k^*$  as a function of  $\lambda$  and  $\tau$  we emphasize that the root changes depending on these variables. The root  $y_k^*$  is found for a given delay  $\tau$  by first calculating the corresponding eigenvalue  $\lambda_k$  and then numerically computing roots of the real part of the characteristic function associated with that eigenvalue,

$$\mathcal{F}_k(y_k^*) = (-y_k^{*2} + \lambda_k\tau^2)^2 \cos y_k^* - \alpha\tau y_k^* \sin y_k^* = 0 \quad (6.7)$$

in the interval  $[\sqrt{\lambda_k\tau^2} - \frac{3\pi}{2}, \sqrt{\lambda_k\tau^2} + \frac{3\pi}{2}]$ . We are only interested in odd roots. If the value  $\sqrt{\lambda_k\tau^2}$  lies within an “odd” interval,  $[j\pi - \pi/2, j\pi + \pi/2]$  for an odd integer  $j$ , the root  $y_k^*$  will also be in this interval. Otherwise, if  $\sqrt{\lambda_k\tau^2}$  is located in an even interval ( $j$  even), the root lies either in the odd interval to the left or to the right. Thus, the supremum of the distance  $|y_k^* - \sqrt{\lambda_k\tau^2}|$  is  $3\pi/2$ . See the appendix for a plot.

It is not a priori identifiable which root  $y_k^*$  dominates stability for which combination of  $\lambda_k$  and  $\tau$ . Therefore, we must conduct the root search for all  $k$  in the transversal set  $\mathcal{N}$ . However, computing these roots with Julia’s `Roots.jl` package [71] goes fast.

### 6.3. Revisiting the star

Let us return to the star topology (figure 6a) as a simple network model that allows us to compare frequency delay with phase delay. Like before, we have a central generator with  $P_+ = 3P_0$  surrounded by three consumers with  $P_- = -P_0$  each. They are connected via lines with homogenous capacity  $K_0$ . We adopt parameter values chosen by Schäfer et al. [48, 56] to allow comparison with their results, too. The values are  $P_0 = 1 \text{ s}^{-2}$ ,  $K_0 = 8 \text{ s}^{-2}$ ,  $\alpha = 0.1 \text{ s}^{-1}$ , and  $\gamma = 0.25 \text{ s}^{-1}$ . This leads to delay stability curves shown in figure 12.

**Stability of the star topology.** Due to the symmetry of the star network,  $\lambda_2 = \lambda_3$ . Figure 12 reveals qualitatively different stability curves for the different eigenvalues  $\lambda_k$ . The eigenvalue  $\lambda_1 = 0$  remains in the stable region until about 9 s and remains unstable thereafter. The non-zero eigenvalues exhibit alternating regimes of stability and instability on the  $\tau$  axis. For the fixed point to be stable at a certain  $\tau$ , all curves must be negative at that point. We note that as in the droop-controlled inverter model of the previous section, the system has a stable fixed point in the absence of delay. Similar to the previous case, there exists a stable region for small  $\tau$ , ranging from  $\tau = 0$  to around  $\tau_1 \approx 340 \text{ ms}$ . This stability region is already significantly longer compared to the droop-controlled inverter model. In contrast to the case of phase delays, the system has further regions (pockets) of stability for larger  $\tau$ , namely the intervals (1.92 s, 2.53 s), (4.19 s, 4.71 s), as well as (6.47 s, 6.90 s). The critical delays are calculated by finding zeros of the delay master stability function  $\sigma$ . (6.6). As before (5.17), the fixed point can be obtained

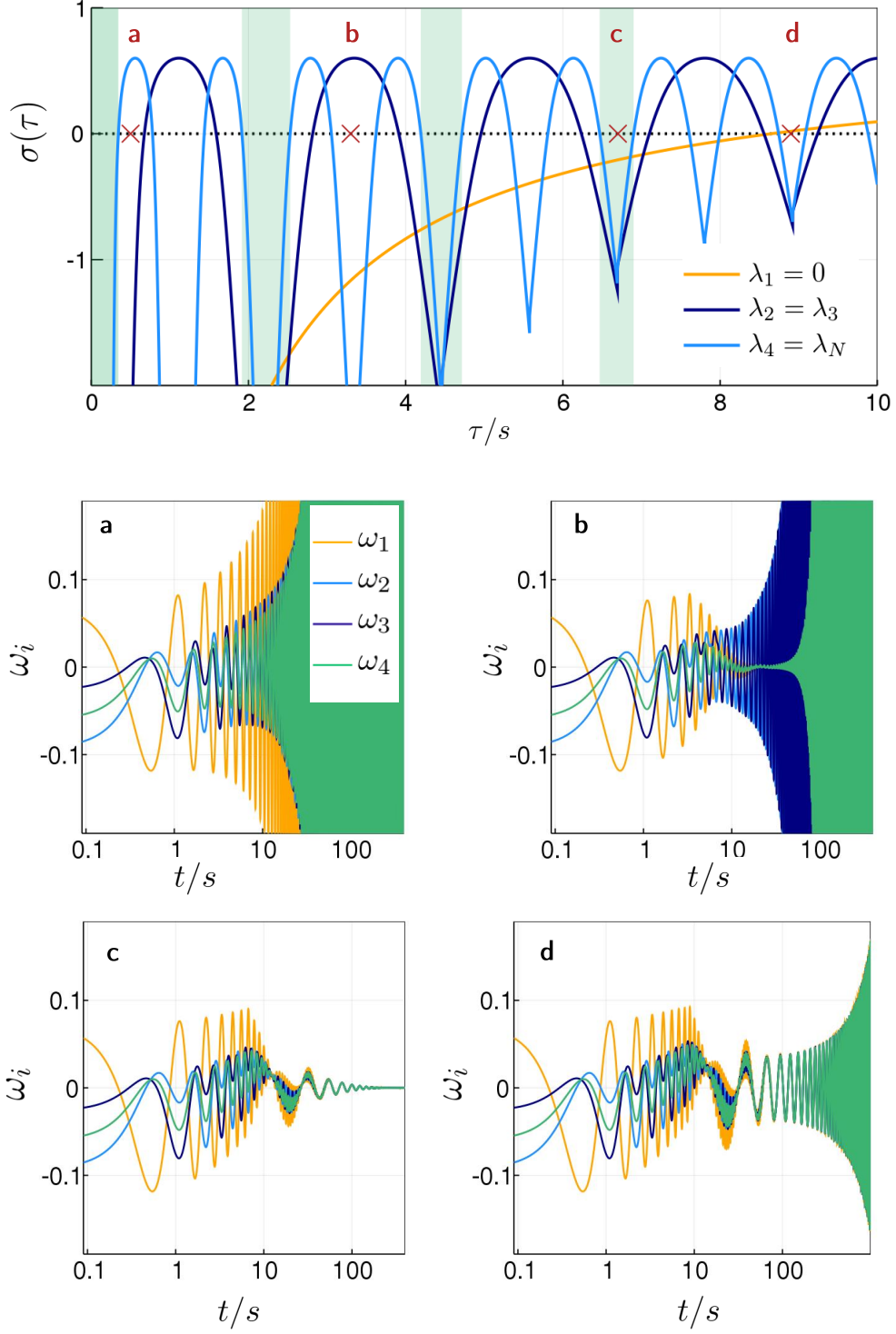


**Figure 12: Stability with frequency delay on the star topology.** Top: The delay master stability function  $\sigma(\tau)$  of the decentral smart grid control model is plotted as a function of the delay for each eigenvalue of the effective Laplacian matrix  $\mathcal{L}$ . The green shaded areas depict regimes of stability. For all other values of  $\tau$ , the system is unstable because at least one of the stability curves is positive. The yellow curve, corresponding to  $\lambda_1 = 0$ , crosses the zero line (black dots) at around 9s and remains positive thereafter. Thus, the four stable pockets are the only stable regions for all  $\tau$ . Bottom: The plots (a,b,c,d) show frequency dynamics of the system after a random perturbation for the delays  $\tau_a = 0.5s$ ,  $\tau_b = 3.3s$ ,  $\tau_c = 6.7s$ ,  $\tau_d = 8.9s$  indicated by red crosses in the top subfigure. The angular frequency deviations of nodes in the star network are plotted on a logarithmic time scale. Parameter values are  $P_0 = 1 \text{ s}^{-2}$ ,  $K_0 = 8 \text{ s}^{-2}$ ,  $\alpha = 0.1 \text{ s}^{-1}$ , and  $\gamma = 0.25 \text{ s}^{-1}$ .

analytically for the star topology; the corresponding spectrum of  $\lambda_k$  is computed numerically in Julia. We obtain

$$\lambda_1 = 0 , \quad \lambda_2 = \lambda_3 \approx 7.94 \text{ s}^{-2} , \quad \lambda_N \approx 31.75 \text{ s}^{-2} .$$

Beyond the point where  $\sigma(\lambda_1, \tau)$  becomes positive, the fixed point is always unstable. Importantly, figure 12 shows that different eigenvalues dominate stability for different values of  $\tau$ .

To verify this result, we run simulations for interesting delay values. In figure 12, plot (a) shows the frequency dynamics of all nodes in a region where  $\lambda_N$  causes instability. The second subfigure (b) depicts instability due to the eigenvalues  $\lambda_{2,3}$ . Furthermore, we simulate the frequency dynamics in the last stable pocket, as shown in (c). The plot (d) highlights that since we have a delay in the isolated dynamics, the zero eigenvalue can contribute to instability. Examining the simulation results in figure 12 also reveals interesting transient behavior not observed in the previous case of phase delays. Specifically, according to subplots (c) and (d), the frequencies align with a frequency oscillating around zero after roughly 10 seconds. In a stable regime, this common oscillation around the synchronous steady state damps out, and the equilibrium is reestablished.

Schäfer et al. [48] obtained agreeing results based on a purely numerical analysis. Thus, our approach provides analytical conditions to confirm their investigation.

With the delay master stability function (6.6) at hand, studying the stability under variation of dynamical parameters or the network structure can be conveniently mastered. We do not pursue this here for the sake of brevity and time.

## 6.4. Back to the roots

To conclude our investigation, let us think back to the initial problem of linear stability analysis for DDEs. In section 2, we discussed that the characteristic function  $\mathcal{H}$  of a delay system poses challenges because it has an infinite number of complex roots. The study of Bhatt and Hsu, based on Pontrjagin's work, aimed at identifying a finite subset of these roots that determines the stability of the system. In practice, these are the roots  $y_1$  for phase delays or the set of  $y_k^*$  or  $y_k^{**}$  for frequency delays. It would be interesting to see how the delay master stability function, given in terms of these critical roots, relates to the real parts of the roots of the characteristic function. To realize this, we take the simplest system possible consisting of only one producer linked to one consumer in power flow equilibrium. This model has been studied in [56]. With decentral smart grid control the dynamics are governed by

$$\Delta\ddot{\phi} = 2P_0 - \alpha\Delta\dot{\phi} - 2K_0 \sin(\Delta\phi) - \gamma\Delta\dot{\phi}^\tau , \quad (6.8)$$

where  $\Delta\phi$  is the phase difference between the two nodes. We take the same parameter values as above. The associated characteristic equation reads

$$\mathcal{H}(z) = z^2 + \alpha z + 2K_0 \cos(\Delta\phi^*) + z\gamma e^{-z\tau} = 0 . \quad (6.9)$$

Figure 13 shows a comparative plot of the real parts of the roots of  $\mathcal{H}$  and the delay master stability function  $\sigma(\tau)$ . The important part is that the delay master stability function accurately reproduces the position of  $\text{Re}(z)$  near the real axis ( $\text{Re}(z) = 0$ ). The figure shows that this is achieved.

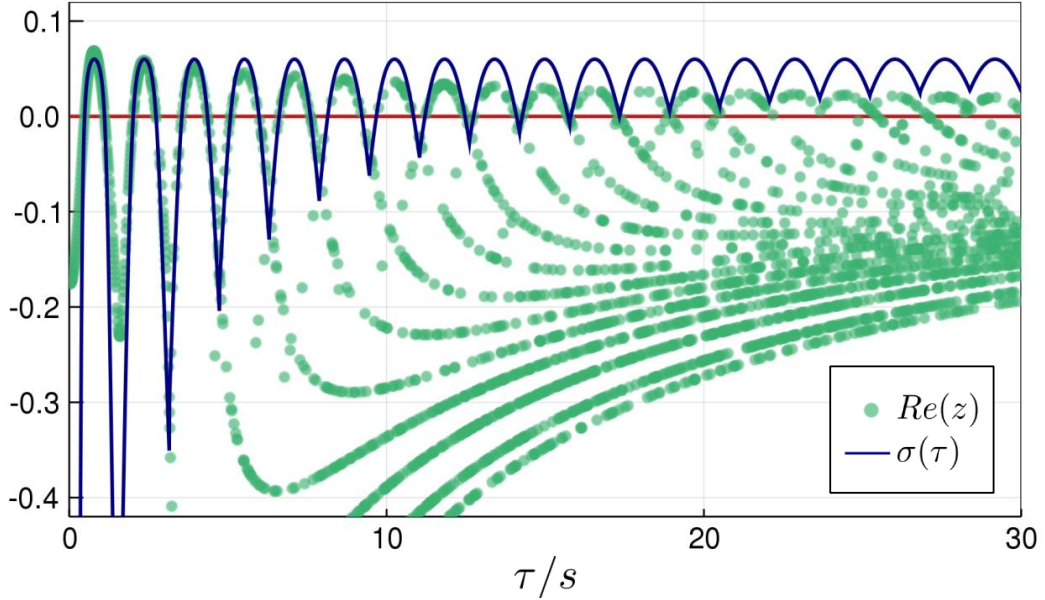


Figure 13: **Spectrum vs. delay master stability function.** Comparative plot of the delay master stability function  $\sigma(\tau)$  and the real parts of 3000 roots  $z$  of the characteristic function  $\mathcal{H}$  (6.8) for the two-node model. The roots are found numerically with random starting values picked from the interval  $(0,1)$ . One root is computed for each  $\tau$  in steps of 0.01s. The red line highlights the axis  $\text{Re}(z) = 0$  where  $\sigma$  must coincide with the spectrum to deliver correct stability conditions. Parameter values are  $P_0 = 1 \text{ s}^{-2}$ ,  $K_0 = 8 \text{ s}^{-2}$ ,  $\alpha = 0.1 \text{ s}^{-1}$ , and  $\gamma = 0.25 \text{ s}^{-1}$ .

## 7. Discussion

After our analysis of two concrete power grid examples, let us reflect upon the general applicability of the delay master stability approach derived in section 3. The starting point of our method is a network of coupled oscillators with delay. The model considers inertia, leading to a second-order form. Apart from inhomogeneous time-independent driving forces, which represent the equilibrium power feed-in in the energy grid models, we consider identical oscillators with equal inertia and damping. As the droop-controlled inverter model exemplifies, these parameters may be tuned by setting distinct droop constants; yet the ratio of the parameters must remain constant, resulting in homogenous *effective* inertia and damping. The limitation to identical dynamical functions at all nodes is certainly an approximation. However, systems of identical oscillators like the Kuramoto model allow rich mathematical analysis [33, 37] and have therefore been widely implemented to study real-world problems. The second-order Kuramoto model is just one popular example of models that are amenable to our method. In principle, our approach allows a much wider range of nonlinear functions for local and coupling dynamics.

Equation (3.2) starts out relatively general by allowing sums of processing and communication delays. However, communication delays turn out to be tricky and require separate treatment. The derivation of our delay master stability approach is based on a number of assumptions on the dynamical functions. We require these assumptions for the following reasons. Our approach follows the idea of the master stability formalism to break down the system of  $N$  DDEs into  $N$  separate blocks. In the traditional master stability formalism [26], the problem immediately has a Kronecker product form because the fixed points are restricted to the complete synchronization manifold. Here, we consider the more general case of frequency synchronization, where all frequencies synchronize but there might be phase differences between nodes. With our assumptions, we achieve the decomposition via Kronecker products, which separate global network information from local dynamics. Moreover, the assumptions then permit applying the Bhatt-Hsu conditions [27].

For processing delays, assumption 1 (antisymmetric coupling) leads to the Laplacian form. Antisymmetric coupling covers a wide range of systems, since diffusion or flow networks fall in this category. Assumption 2 (homogeneity of local Jacobians) rules out that the derivatives of the local functions  $f^0$  and  $f^\tau$  depend on the fixed point. Furthermore, the third assumption (factorizability of coupling Jacobians) restricts the choice of coupling functions  $g^{00}$  and  $g^{\tau\tau}$ . The purpose of assumptions 2 and 3 is to ensure that all matrices on the global level of the Kronecker products commute. Then, they are simultaneously diagonalizable. In most cases, assumption 3 boils down to the requirement that the system is either coupled only via the phase or only via the frequency. This relates to assumption 4 (single delay term), which prohibits the coexistence of phase and frequency delays.

Interestingly, Bhatt and Hsu point out in the end of [27] that their stability analysis could evidently be transferred to systems involving more than one time lag term, meaning that phase and frequency delay could coexist. Thus, assumption 4 might become dispensable in the long-run.

For increased clarity, we presented the derivation for pure coupling processing delays given by the function  $g^{\tau\tau}$  and argued that the procedure is analogous for undelayed coupling ( $g^{00}$ ). In fact, it would also be possible to have a sum of both functions, as long as both satisfy assumption 3 and lead to the same effective adjacency matrix  $\mathcal{A}$ .

Communication delays cannot be expressed in the Laplacian form because the arguments of the function  $g^{0\tau}$  are evaluated at different times ( $x_i(t), x_j(t - \tau)$ ). The derivation of the asymmetric case (section 3.3) is admittedly enforced to work by imposing hypothetical assumptions. In practice, assumption 6 only clearly holds for regular graphs and complete synchronization. For this reason, our method is mainly useful for processing delays, and we present the derivation of communication delays rather for the sake of completeness.

Our approach delivers analytical necessary and sufficient conditions for stability with delay. Nonetheless, we may have to test the analytical stability condition with numerical tools. The

fixed point is usually obtained numerically, and also finding the wanted roots of the characteristic function  $\mathcal{F}$  or  $\mathcal{G}$  requires numerical calculations. For the case of phase delay, determining the root  $y_1$  is straight-forward and independent of  $k$ . Conversely, for frequency delays, the fitting root must be found separately for each eigenvalue  $\lambda_k$ . However, we can narrow down the interval in which the respective root lies; we must therefore calculate at maximum  $2N$  roots. Deeper analysis of the roots  $y^*$ ,  $y^{**}$  might reduce this number further.

The master stability formalism aims at obtaining a master stability condition which contrasts the eigenvalue  $\lambda_k$  with dynamical parameters of the system. In the case of a coupling processing delay in the phase, illustrated by the droop-controlled inverter model, this is conveniently achieved. However, the stability conditions for the other cases comprise more tangled expressions, and it is generally not possible to clearly separate network information from dynamical information on opposite sides of an inequality. This remains a “cosmetic” flaw, though, because we still obtain exact conditions which state fairly simple requirements for the parameters of the system. For the systems considered in this thesis, computation times were usually fast even on an old personal computer.

Our delay stability analysis of two power grid models serves the primary purpose of verifying and illustrating our delay master stability approach. Obviously, the network structures considered in this thesis do not reproduce the complex, amorphous structure of real-world energy systems, today and in the future. Also, we neglect line losses, reactive power flows and time-dependent voltage amplitudes (these are common approximations in the literature).

Nonetheless, our analysis allows some conclusions about how delays affect the stability of synchronous states in power grids. For a coupling processing delay in the phase, there exists a critical delay which marks the upper bound of a delay stability window. Physically, we interpret this in the following way. The delayed coupling term acts as a time-dependent driving term. For small delays, it fulfills the purpose of droop control to damp out perturbations. If the delay becomes too large, however, the droop control kicks in too late to stabilize frequency deviations. Instead, it acts on the basis of “too old” power flow information and fails as a control. The study of Watts-Strogatz small-world networks produces intuitive results. Large system sizes and high degrees of randomness diminish delay stability. Basically, more complex structures require smaller delays to remain stable. We infer that this is because complex interactions can amplify the destabilizing effect of delayed reactions.

We illustrate the case of frequency delays with the example of decentral smart grid control (local processing delay). Unlike the previous case, our results show that there exists several stability regimes in certain  $\tau$ -intervals. This confirms the numerical analysis carried out by Schäfer et al. [48, 56]. As the authors explain, the price adaptation term contributes a time-dependent driving force which can either damp out or magnify perturbations, depending on whether it acts in phase or out of phase. With growing delay, the stability regimes get smaller until instability persists because the price adaptation kicks in too late to achieve a re-stabilizing effect. While we assume here that the synchronous fixed points are stable in the absence of delay, Schäfer et al. show that averaging over a time interval in the past can have a stabilizing effect. To investigate this further, it would be desirable to expand our approach to multiple delays.

In any case, power grids are a relevant application of our delay stability method, since control units always incorporate a processing delay for technical reasons. Communication delays do not play a significant role in frequency control of power systems unless a smart grid with an extensive communication network parallel to the power grid is considered.

To conclude, we stress the fact that linear stability is a local measure which yields information about the systems asymptotic behavior after small perturbations. In power grids and other real-world systems, perturbations may certainly be large, and the transient behavior might play a role. This requires global stability measures.

## 8. Conclusion and Outlook

As a science that combines mathematics with the exploration of natural phenomena, physics often builds the bridge between theory and application. In the first part of this thesis, we derive an approach to assess the linear stability of a complex network of  $N$  coupled inertial oscillators with delay. The system is described as a set of nonlinear second-order delay differential equations. We consider identical oscillators with the slight generalization that their dynamics may be driven by differing constant inhomogeneities. Our method investigates how a constant delay  $\tau$ , which may appear in the local dynamics as well as in the coupling term, affects the stability of synchronized states. Based on the master stability formalism and adopting results from Bhatt and Hsu, we state necessary and sufficient criteria for linear stability with any delay  $\tau > 0$ . While MSF and the Bhutt-Hsu conditions exist for a while already, the combination and generalization performed here yields interesting and practical new results.

The analysis concentrates on processing delays with asymmetric coupling which allows to project the linearized state vector into the eigenspace of the Laplacian matrix. In this case, the conditions depend on the delay, the Laplacian eigenvalues  $\lambda_k$ , linearized dynamical parameters of the nodes as well as maximally  $2N$  uniquely defined roots  $z$  of the characteristic equation as a function of  $\tau$ . We distinguish between phase delays and frequency delays, which leads to qualitatively different criteria. In the case of communication delays or other asymmetric coupling, our derivation requires a strongly restrictive assumption.

In the second part of this thesis, we apply our method to two simple models of renewable power grids. Stabilizing the grid frequency becomes increasingly important as the energy landscape undergoes a fundamental transition from synchronous generators to volatile distributed generation sources. Future control units may exhibit a non-negligible processing delay.

The first example considers a phase delay in the coupling of grid-forming inverters adopted from Schiffer et al. We show that there exists a critical delay  $\tau_c$  above which the system destabilizes. Analyses of small-world Watts-Strogatz networks reveal that increasing complexity diminishes delay stability. The results are verified with simulations. Secondly, we study a frequency delay in the local dynamics of decentral smart grid control. Here, several regimes of stability appear. Our results accord with numerical investigations by Schäfer et al.

Due to its increasing importance in real-world applications, the delay stability of synchronous oscillator networks remains a hot topic in research. These systems are tricky due to the infinite dimensionality of delay differential equations as well as rich emergent dynamical behavior caused by complex interactions. Further research is in need to tackle non-identical oscillators, to consider more than one delay, or to derive more general criteria particularly for communication delays. Whether delays can also act in a stabilizing way poses one of many interesting questions that motivate to dig deeper.



## Appendix

### A. Derivation of the droop-controlled inverter model with delay

In section 5.1 we analyze a modified version of the droop-controlled inverter model introduced by Schiffer et al. [52]. Here we outline how equation (5.1) follows from the original description<sup>11</sup>. Schiffer et al. propose a control scheme for grid-forming inverters with AC voltage  $V_i(t) = U_i(t) \exp\{i\phi_i(t)\}$ , modelled by

$$\begin{aligned}\dot{\phi}_i &= u_i^\phi \\ \tau_i^V \dot{U}_i &= -U_i + u_i^V\end{aligned}\tag{A.1}$$

with proportional control inputs

$$\begin{aligned}u_i^\phi &= \Omega - \beta_i^P (P_i^m - P_i^d) \\ u_i^V &= U_i^d - \beta_i^Q (Q_i^m - Q_i^d) \\ \tau_i^P \dot{P}_i^m &= -P_i^m + P_i(U, \phi) \\ \tau_i^P \dot{Q}_i^m &= -Q_i^m + Q_i(U, \phi).\end{aligned}\tag{A.2}$$

Here, the superscript  $m$  indicates measured quantities, whereas the superscript  $d$  denotes desired set points.  $P$  and  $Q$  represent active and reactive powers, respectively;  $\Omega$  is the nominal grid frequency and  $\beta_i^P$ ,  $\beta_i^Q$  denote droop gains for active and reactive power. Furthermore,  $\tau_i^V$  and  $\tau_i^P$  are the time constants of low-pass filters which represent delays caused by measuring and processing power data.

As before, we assume that dynamical changes affect mainly the phase, such that the voltage amplitude may be approximated as constant (phase approximation [33]). Thus we set  $\dot{U}_i = 0$ , leading to the closed-loop system (see [52])

$$\begin{aligned}\dot{\phi}_i &= \omega_i \\ \tau_i^P \dot{\omega}_i &= -\omega_i + \Omega - \beta_i^P (P_i(\phi) - P_i^d).\end{aligned}\tag{A.3}$$

We argue that instead of representing the processing delays by low-pass filters with time constants  $\tau_i^P$ , we might as well use a DDE form where the power  $P_i(\phi)$  is a delayed function of the phase. To do this, we replace  $\tau_i^P$  in (A.3) by a delay  $\tau_i$  appearing in the phase:

$$\dot{\omega}_i = -\omega_i + \Omega - \beta_i^P (P_i(\phi(t - \tau_i)) - P_i^d).\tag{A.4}$$

Moreover, we assume that all inverters have the same time lag, i.e.  $\tau_i \equiv \tau \forall i$ . Switching to a reference frame co-rotating with the frequency  $\Omega$  and adding inertia and damping prefactors  $m_i$ ,  $\alpha_i$  for more generality, we have

$$\begin{aligned}\dot{\phi}_i &= \omega_i \\ m_i \dot{\omega}_i &= -\alpha_i \omega_i - \beta_i^P (P_i(\phi(t - \tau)) - P_i^d),\end{aligned}\tag{A.5}$$

which is precisely equation (5.1).

<sup>11</sup>The derivation is based on unpublished work by the group “Dynamics, stability and resilience of complex hybrid infrastructure networks” at the Potsdam Institute for Climate Impact Research (PIK), specifically P. Schultz, B. Ünzelmann, and F. Hellmann.

## B. The roots $y_k^*$

We return to the decentral smart grid control model on the star topology in section 6. Although, as mentioned, finding the right roots  $y_k^*$  is a bit more elaborate than in the phase delay case, we know a priori in which interval the wanted root lies for a given  $\tau$ . Here, we illustrate this by an explicit plot (figure 14).

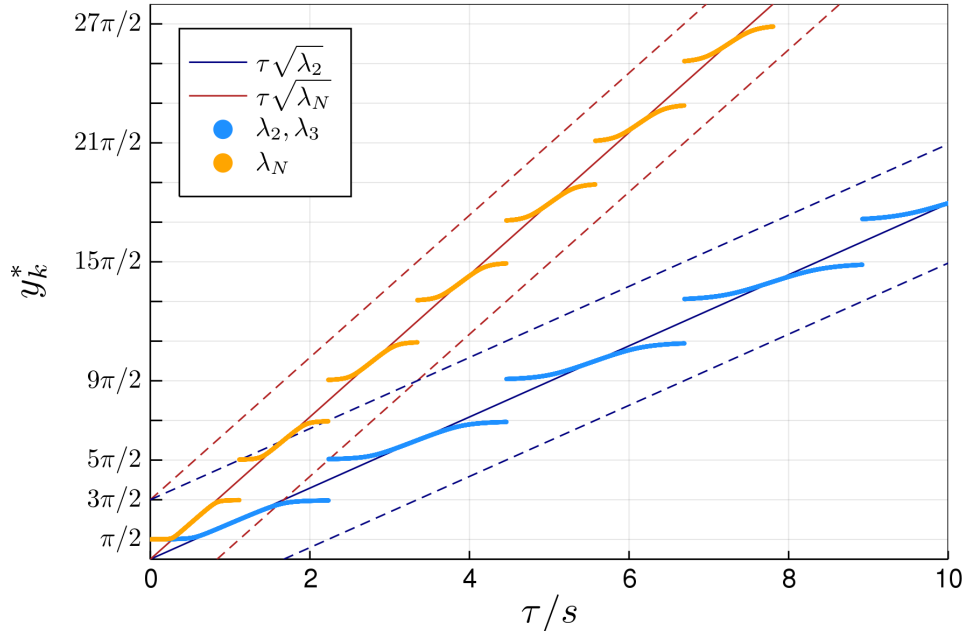


Figure 14: **Wanted roots as a function of delay.** Scatter plot of the roots  $y_2^*$  (blue dots) and  $y_N^*$  (orange dots) from  $\tau = 0$  to  $\tau = 10$  s. The roots only lie in odd intervals  $(j\pi - \pi/2, j\pi + \pi/2)$ ,  $j$  odd. The solid lines show the value  $\sqrt{\lambda_k \tau^2}$  for  $k = 2$  (blue) and  $k = N$  (red), which plays a role in determining the stability-defining root (see sections 3 and 6). The dotted lines have a vertical distance of  $3\pi/2$  from the corresponding solid line, thus bordering the interval where the root could be found. As the plot shows, the roots are actually even closer to the value  $\sqrt{\lambda_k \tau^2}$ . Parameter values for the calculation are  $P_0 = 1 \text{ s}^{-2}$ ,  $K_0 = 8 \text{ s}^{-2}$ ,  $\alpha = 0.1 \text{ s}^{-1}$ , and  $\gamma = 0.25 \text{ s}^{-1}$ .

## C. Behind the scenes

Plots were made in Julia using `Plots.jl`. As a helpless programming novice, I am proud to admit that the arrangement of multiple figures, convenient positioning of legends as well as the flow chart were all done in Microsoft PowerPoint. Graph plots were enhanced in Gimp2.

## References

- [1] Kuang, Y. *Delay differential equations: with applications in population dynamics*. Vol. 191. Academic press, 1993.
- [2] Keane, A, Krauskopf, B, and Postlethwaite, CM. “Climate models with delay differential equations”. In: *Chaos: An Interdisciplinary Journal of Nonlinear Science* 27.11 (2017), p. 114309.
- [3] Erneux, T, Javaloyes, J, Wolfrum, M, and Yanchuk, S. “Introduction to Focus Issue: Time-delay dynamics”. In: *Chaos: An Interdisciplinary Journal of Nonlinear Science* 27.11 (2017), p. 114201. DOI: 10.1063/1.5011354.
- [4] Soriano, MC, Garcia-Ojalvo, J, Mirasso, CR, and Fischer, I. “Complex photonics: Dynamics and applications of delay-coupled semiconductors lasers”. In: *Reviews of Modern Physics* 85.1 (2013), p. 421.
- [5] Ruschel, S and Yanchuk, S. “Chaotic bursting in semiconductor lasers”. In: *Chaos: An Interdisciplinary Journal of Nonlinear Science* 27.11 (2017), p. 114313. DOI: 10.1063/1.5007876.
- [6] Orosz, G, Wilson, RE, and Stépán, G. *Traffic jams: dynamics and control*. 2010.
- [7] Sipahi, R, Lämmer, S, Helbing, D, and Niculescu, SI. “On stability problems of supply networks constrained with transport delay”. In: *Journal of dynamic systems, measurement, and control* 131.2 (2009), p. 021005.
- [8] Bellman, RE and Cooke, KL. *Differential-Difference Equations*. Rand Corporation, Santa Monica, CA, 1963.
- [9] Diekmann, O, Gils, S van, Lunel, S, and Walther, H. *Delay Equations: Functional-, Complex-, and Nonlinear Analysis*. Springer, 2012.
- [10] Roussel, M. *Delay-differential equations*. 2005. URL: <http://people.uleth.ca/~roussel/nld/delay.pdf> (visited on 03/13/2019).
- [11] Humphries, T. *Delay Differential Equations*. Lecture at the NZMRI Summer School on Continuation Methods in Dynamical Systems. 2016. URL: <https://www.math.auckland.ac.nz/~hinke/meetings/NZMRI/materials/NZMRI16-Tony1.pdf> (visited on 03/13/2019).
- [12] Ruan, S and Wei, J. “On the zeros of transcendental functions with applications to stability of delay differential equations with two delays”. In: *Dynamics of Continuous Discrete and Impulsive Systems Series A* 10 (2003), pp. 863–874.
- [13] Airy, GB. *On certain Conditions under which a Perpetual Motion is possible*. J. Smith, 1830.
- [14] Newman, M. *Networks. An Introduction*. Oxford University Press, 2010.
- [15] Kuramoto, Y. “Self-entrainment of a population of coupled non-linear oscillators”. In: *International symposium on mathematical problems in theoretical physics*. Springer. 1975, pp. 420–422.
- [16] Nishikawa, T and Motter, AE. “Comparative analysis of existing models for power-grid synchronization”. In: *New Journal of Physics* 17.1 (2015), p. 015012.
- [17] International Energy Agency. *Renewables Information: Overview*. 2018. URL: <https://webstore.iea.org/renewables-information-2018>.
- [18] Kroposki, B, Johnson, B, Zhang, Y, Gevorgian, V, Denholm, P, Hodge, BM, and Hannegan, B. “Achieving a 100% renewable grid: Operating electric power systems with extremely high levels of variable renewable energy”. In: *IEEE Power and Energy Magazine* 15.2 (2017), pp. 61–73.

- [19] Schiffer, J, Zonetti, D, Ortega, R, Stankovic, A, Sezi, T, and Raisch, J. “A survey on modeling of microgrids - from fundamental physics to phasors and voltage sources”. In: (2015). arXiv: <http://arxiv.org/abs/1505.00136v2>.
- [20] Anvari, M, Lohmann, G, Wächter, M, Milan, P, Lorenz, E, Heinemann, D, Tabar, MRR, and Peinke, J. “Short term fluctuations of wind and solar power systems”. In: *New Journal of Physics* 18.6 (2016), p. 063027.
- [21] Ueckerdt, F, Brecha, R, and Luderer, G. “Analyzing major challenges of wind and solar variability in power systems”. In: *Renewable energy* 81 (2015), pp. 1–10.
- [22] Maia, D, Macau, EE, Pereira, T, and Yanchuk, S. “Synchronization in Networks with Strongly Delayed Couplings”. In: *arXiv preprint arXiv:1711.03422* (2017).
- [23] Sieber, J, Wolfrum, M, Lichtner, M, and Yanchuk, S. “On the stability of periodic orbits in delay equations with large delay”. In: *Discrete and Continuous Dynamical Systems - Series A* 33(7), 3109–3134, 2013 (2011). DOI: [10.3934/dcds.2013.33.3109](https://doi.org/10.3934/dcds.2013.33.3109).
- [24] Lichtner, M, Wolfrum, M, and Yanchuk, S. “The Spectrum of Delay Differential Equations with Large Delay”. In: *SIAM Journal on Mathematical Analysis* 43.2 (2011), pp. 788–802. DOI: [10.1137/090766796](https://doi.org/10.1137/090766796).
- [25] Ruschel, S. *The spectrum of linear delay differential equations with multiple hierarchical large delays*. Group Seminar, Technische Universität Berlin. 2018.
- [26] Pecora, L and Carroll, T. “Master Stability Functions for Synchronized Coupled Systems”. In: *Phys. Rev. Lett.* 80.10 (Mar. 1998), pp. 2109–2112. DOI: [10.1103/PhysRevLett.80.2109](https://doi.org/10.1103/PhysRevLett.80.2109).
- [27] Bhatt, S and Hsu, C. “Stability criteria for second-order dynamical systems with time lag”. In: *Journal of Applied Mechanics* 33.1 (1966), pp. 113–118.
- [28] Arnold, V. *Ordinary Differential Equations*. Trans. by Cooke, R. Springer, 1992.
- [29] Buchanan, J. *The existence and uniqueness of solutions to differential equations*. 2010. URL: <http://www.math.uchicago.edu/~may/VIGRE/VIGRE2010/REUPapers/Buchanan.pdf> (visited on 03/13/2019).
- [30] Hellmann, F and Schultz, P. “Complex Network Dynamics”. Lecture notes. Humboldt-Universität Berlin, 2019.
- [31] Jarlebring, E. “The spectrum of delay-differential equations: numerical methods, stability and perturbation”. PhD thesis. 2008.
- [32] Arenas, A, Díaz-Guilera, A, Kurths, J, Moreno, Y, and Zhou, C. “Synchronization in complex networks”. In: *Physics Reports* 469.3 (2008), pp. 93–153.
- [33] Pikovsky, A, Rosenblum, M, and Kurths, J. *Synchronization: a universal concept in nonlinear sciences*. Vol. 12. Cambridge university press, 2003.
- [34] Buck, JB. “Synchronous rhythmic flashing of fireflies”. In: *The Quarterly Review of Biology* 13.3 (1938), pp. 301–314.
- [35] Wiesenfeld, K, Colet, P, and Strogatz, SH. “Synchronization transitions in a disordered Josephson series array”. In: *Physical review letters* 76.3 (1996), p. 404.
- [36] Eckhardt, B, Ott, E, Strogatz, SH, Abrams, DM, and McRobie, A. “Modeling walker synchronization on the Millennium Bridge”. In: *Physical Review E* 75.2 (2007), p. 021110.
- [37] Rodrigues, FA, Peron, TKD, Ji, P, and Kurths, J. “The Kuramoto model in complex networks”. In: *Physics Reports* 610 (2016), pp. 1–98.
- [38] Acebrón, JA, Bonilla, LL, Vicente, CJP, Ritort, F, and Spigler, R. “The Kuramoto model: A simple paradigm for synchronization phenomena”. In: *Reviews of modern physics* 77.1 (2005), p. 137.

- [39] Yeung, MS and Strogatz, SH. “Time delay in the Kuramoto model of coupled oscillators”. In: *Physical Review Letters* 82.3 (1999), p. 648.
- [40] Pontrjagin, L. “On the Zeros of Some Elementary Transcendental Functions”. In: *American Mathematical Society Translations*. 2nd ser. 1 (1955), pp. 95–110.
- [41] Pontrjagin, L. “On the Zeros of Some Transcendental Functions”. In: *American Mathematical Society Translations*. 2nd ser. 8 (1958), pp. 19–20.
- [42] Hörsch, J, Hofmann, F, Schlachtberger, D, and Brown, T. “PyPSA-Eur: An open optimisation model of the European transmission system”. In: *Energy strategy reviews* 22 (2018), pp. 207–215.
- [43] Machowski, J, Bialek, J, and Bumby, J. *Power system dynamics: stability and control*. John Wiley & Sons, 2011.
- [44] E, L and E, H. *Electricity distribution network design. 2nd Edition*. Peter Peregrinus Ltd., 1995.
- [45] Schultz, P, Hellmann, F, Heitzig, J, and Kurths, J. “A Network of Networks Approach to Interconnected Power Grids”. In: *arXiv:1701.06968* (2016).
- [46] Amprion. *Der Weg des Stroms vom Kraftwerk zum Verbraucher*. URL: <https://www.amprion.net/%C3%9Cbertragungsnetz/Weg-des-Stroms/> (visited on 03/21/2019).
- [47] Short, JA, Infield, DG, and Freris, LL. “Stabilization of grid frequency through dynamic demand control”. In: *IEEE Transactions on power systems* 22.3 (2007), pp. 1284–1293.
- [48] Schäfer, B, Grabow, C, Auer, S, Kurths, J, Witthaut, D, and Timme, M. “Taming instabilities in power grid networks by decentralized control”. In: *The European Physical Journal Special Topics* 225.3 (2016), pp. 569–582. DOI: [10.1140/epjst/e2015-50136-y](https://doi.org/10.1140/epjst/e2015-50136-y).
- [49] Alipoor, J, Miura, Y, and Ise, T. “Power system stabilization using virtual synchronous generator with alternating moment of inertia”. In: *IEEE Journal of Emerging and Selected Topics in Power Electronics* 3.2 (2015), pp. 451–458.
- [50] Tayyebi, A, Groß, D, Anta, A, Kupzog, F, and Dörfler, F. “Interactions of Grid-Forming Power Converters and Synchronous Machines—A Comparative Study”. In: *arXiv preprint arXiv:1902.10750* (2019).
- [51] Mohd, A, Ortjohann, E, Sinsukthavorn, W, Lingemann, M, Hamsic, N, and Morton, D. “Supervisory control and energy management of an inverter-based modular smart grid”. In: *2009 IEEE/PES Power Systems Conference and Exposition*. IEEE. 2009, pp. 1–6.
- [52] Schiffer, J, Ortega, R, Astolfi, A, Raisch, J, and Sezi, T. “Conditions for stability of droop-controlled inverter-based microgrids”. In: *Automatica* 50.10 (2014), pp. 2457–2469.
- [53] Beck, HP and Hesse, R. “Virtual synchronous machine”. In: *2007 9th International Conference on Electrical Power Quality and Utilisation*. IEEE. 2007, pp. 1–6.
- [54] Serban, I and Ion, CP. “Microgrid control based on a grid-forming inverter operating as virtual synchronous generator with enhanced dynamic response capability”. In: *International Journal of Electrical Power & Energy Systems* 89 (2017), pp. 94–105.
- [55] Driesen, J and Visscher, K. “Virtual synchronous generators”. In: *2008 IEEE Power and Energy Society General Meeting-Conversion and Delivery of Electrical Energy in the 21st Century*. IEEE. 2008, pp. 1–3.
- [56] Schäfer, B, Matthiae, M, Timme, M, and Witthaut, D. “Decentral Smart Grid Control”. In: *New Journal of Physics* 17.1 (2015), p. 015002. DOI: [10.1088/1367-2630/17/1/015002](https://doi.org/10.1088/1367-2630/17/1/015002).
- [57] Wang, J, Yan, JD, Jiang, L, and Zou, J. “Delay-Dependent Stability of Single-Loop Controlled Grid-Connected Inverters withLCLFilters”. In: *IEEE Transactions on Power Electronics* 31.1 (2016), pp. 743–757.

- [58] Hellmann, F, Schultz, P, Jaros, P, Levchenko, R, Kapitaniak, T, Kurths, J, and Maistrenko, Y. “Network-induced multistability: Lossy coupling and exotic solitary states”. In: *arXiv preprint arXiv:1811.11518* (2018).
- [59] Menck, PJ, Heitzig, J, Kurths, J, and Schellnhuber, HJ. “How dead ends undermine power grid stability”. In: *Nature communications* 5 (2014), p. 3969.
- [60] Holmgren, ÅJ. “Using graph models to analyze the vulnerability of electric power networks”. In: *Risk analysis* 26.4 (2006), pp. 955–969.
- [61] Pagani, GA and Aiello, M. “The power grid as a complex network: a survey”. In: *Physica A: Statistical Mechanics and its Applications* 392.11 (2013), pp. 2688–2700.
- [62] Dörfler, F and Bullo, F. “Kron reduction of graphs with applications to electrical networks”. In: *IEEE Transactions on Circuits and Systems I: Regular Papers* 60.1 (2013), pp. 150–163.
- [63] Dörfler, F and Bullo, F. *Synchronization and Kron Reduction in Power Networks*. Talk at Center for Nonlinear Studies, Los Alamos National Labs. 2011. URL: <https://cnls.lanl.gov/~chertkov/SmarterGrids/Talks/Dorfler.pdf>.
- [64] Dörfler, F and Bullo, F. “Exploring synchronization in complex oscillator networks”. In: *2012 IEEE 51st IEEE Conference on Decision and Control (CDC)*. IEEE. 2012, pp. 7157–7170.
- [65] Meschede, D. *Gerthsen Physik*. Springer-Verlag, 2015.
- [66] In discussion with P. Schultz, based on unpublished work by P. Schultz, B. Ünzelmann, F. Hellmann (2018).
- [67] Huang, W, Lu, M, and Zhang, L. “Survey on microgrid control strategies”. In: *Energy Procedia* 12 (2011), pp. 206–212.
- [68] Engler, A and Soultanis, N. “Droop control in LV-grids”. In: *2005 International Conference on Future Power Systems*. IEEE. 2005, 6–pp.
- [69] Shuai, Z, Mo, S, Wang, J, Shen, ZJ, Tian, W, and Feng, Y. “Droop control method for load share and voltage regulation in high-voltage microgrids”. In: *Journal of Modern Power Systems and Clean Energy* 4.1 (2016), pp. 76–86. DOI: 10.1007/s40565-015-0176-1.
- [70] *LinearAlgebra.jl*. URL: <https://github.com/JuliaLang/julia/tree/master/stdlib/LinearAlgebra> (visited on 04/07/2019).
- [71] *Roots.jl*. URL: <https://github.com/JuliaMath/Roots.jl> (visited on 04/07/2019).
- [72] Rackauckas, C and Nie, Q. “Differentialequations.jl – a performant and feature-rich ecosystem for solving differential equations in Julia”. In: *Journal of Open Research Software* 5.1 (2017).
- [73] Watts, DJ and Strogatz, SH. “Collective dynamics of ‘small-world’ networks”. In: *nature* 393.6684 (1998), p. 440.
- [74] Del Sol, A and O’Meara, P. “Small-world network approach to identify key residues in protein–protein interaction”. In: *Proteins: Structure, Function, and Bioinformatics* 58.3 (2005), pp. 672–682.
- [75] Watts, DJ. *The Small World Problem*. Presentation slides. URL: [http://blacky.terra32.net/trusso/CORSO\\_TeoriaAvanzataReti/info4/altrecose/DuncanJWattsSigma.pdf](http://blacky.terra32.net/trusso/CORSO_TeoriaAvanzataReti/info4/altrecose/DuncanJWattsSigma.pdf).
- [76] *LightGraphs.jl*. URL: <https://github.com/JuliaGraphs/LightGraphs.jl> (visited on 04/07/2019).
- [77] *GraphPlot.jl*. URL: <https://github.com/JuliaGraphs/GraphPlot.jl> (visited on 04/07/2019).

---

## Acknowledgements

To begin with, I would like to thank Professor Petra Imhof from Freie Universität Berlin for supervising this thesis in the middle of preparations to move to Norway. Thanks to her flexibility and very friendly support, I could embrace the unique opportunity to conduct my research at the Potsdam Institute for Climate Impact Research (PIK).

I would like to express my sincere gratitude to my research supervisor at PIK, Dr. Frank Hellmann. With his helpful advice and continuous support, he guided me through this work from the choice of topic to the final draft. Equal thankfulness goes to Dr. Paul Schultz, who has been extremely supportive and contributed many useful ideas. Anton Plietzsch helped me a lot with getting started in Julia.

Being part of Research Department 4 – Complexity Science at PIK offered much more than an excellent research environment. In the past months, I learned new things far beyond the scope of my thesis. I thank Dr. Hellmann, Dr. Schultz, and everyone in RD4 for inspiring me both academically and personally.

My thanks go out to Anne and Kaja, who refrained from criticizing the increasing entropy in our shared apartment and made tea when they found me sleeping on the kitchen floor.

This thesis is dedicated to all Jupyter kernels that died during its making.

---

## **Declaration of Originality**

I, Reyk Börner, hereby confirm that I have written the present thesis by myself, without contributions from any sources other than those cited in the text. This also applies to all graphics, drawings, maps, and images included in the thesis.

---

Berlin, April 9, 2019

5001531

Date

Matriculation number

Signature